DETERMINATION OF RESPIRATORY AND HEART RATES FROM PPG SIGNALS USING FBSE-EWT METHOD

M.Tech. Thesis

By

RAJAT KATIYAR

DISCIPLINE OF ELECTRICAL ENGINEERING

INDIAN INSTITUTE OF TECHNOLOGY INDORE

JULY 2019

DETERMINATION OF RESPIRATORY AND HEART RATES FROM PPG SIGNALS USING FBSE-EWT METHOD

A THESIS

Submitted in partial fulfillment of the requirements for the award of the degree

of

Master of Technology

in

Electrical Engineering

with specialization in

Communication and Signal Processing

by

RAJAT KATIYAR

DISCIPLINE OF ELECTRICAL ENGINEERING

INDIAN INSTITUTE OF TECHNOLOGY INDORE

JULY 2019

INDIAN INSTITUTE OF TECHNOLOGY INDORE

CANDIDATE'S DECLARATION

I hereby certify that the work which is being presented in the thesis entitled **DETERMINATION OF RESPIRATORY AND HEART RATES FROM PPG SIGNALS USING FBSE-EWT METHOD** in the partial fulfillment of the requirements for the award of the degree of **MASTER OF TECHNOLOGY** and submitted in the **DISCIPLINE OF ELECTRICAL ENGINEERING, Indian Institute of Technology Indore**, is an authentic record of my own work carried out during the time period from July 2018 to July 2019 under the supervision of Prof. Ram Bilas Pachori, Professor, Discipline of Electrical Engineering, IIT Indore.

The matter presented in this thesis has not been submitted by me for the award of any other degree of this or any other institute.

Signature of the student with date
(RAJAT KATIYAR)

This is to certify that the above statement made by the candidate is correct to the best of my/our knowledge.

Signature of the Supervisor of
M.Tech. thesis (with date)
(Prof. Ram Bilas Pachori)

RAJAT KATIYAR has successfully given his M.Tech. Oral Examination held on **01-07-2019.**

Signature(s) of Supervisor(s) of M.Tech. thesis
Date:

Convener, DPGC
Date:

Signature of PSPC Member #1
Date:

Signature of PSPC Member #2
Date:

Acknowledgements

First of all, I would like to express my sincere gratitude to my thesis supervisor **Prof. Ram Bilas Pachori** for his constant support, encouragement and guidance during my Master's study and thesis work. Furthermore, I would like to express my deep gratitude to my PSPC members **Dr. Prabhat Kumar Upadhyay** and **Prof. Anand Parey** for their valuable suggestions and feedback.

I would also like to thank all the faculty members and the staff at IIT Indore for their cooperation throughout my study and thesis work. I would like to thank the Discipline of Electrical Engineering for providing all the facilities, resources, and research environment required for the completion of this work.

I would like to thank all the members of Signal Analysis Research Lab for their assistance at various levels of this work.

I am grateful to all my colleagues for their constant support, fruitful discussions, and making my stay at the institute enjoyable.

I am especially grateful to my family members for their invaluable support and strong belief in me. Their sacrifices and unbounded love motivate me to remain focused and determined, which always pushes me to strive for excellence. I dedicate my Master's thesis to my great parents for their countless sacrifices.

RAJAT KATIYAR
mt1702102006
M.Tech. (Communication and Signal Processing)
Discipline of Electrical Engineering, IIT Indore

Dedicated to my family

Abstract

Respiratory rate (RR) and heart rate (HR) are vital parameters that show signs of abnormal human breathing activity. There are various techniques for extracting RR and HR. In addition to oxygen saturation (SpO2) and cardiac rate measurement, the photoplethysmography (PPG) signal can be used to obtain breathing information that prevents the additional measurement sensor from being used. An algorithm has been suggested for the extraction of RR and HR from PPG signals using Fourier-Bessel series expansion based empirical wavelet transform (FBSE-EWT) in this work. We have taken 310 and 632 epochs of simultaneous recorded PPG and breathing signals from MIMIC and capnobase databases in order to investigate the efficiency of the suggested algorithm. RR extraction from PPG signals by FBSE-EWT shows that the root mean square errors (RMSEs) for both MIMIC and capnobase databases are 0.48549 breaths/minute and 0.92545 breaths/minute. For HR, RMSEs are 2.39632 beats/min and 1.444 beats/min for both MIMIC and capnobase databases, respectively. These findings show that the suggested FBSE-EWT method is more accurate in estimating RR in comparison to other existing techniques.

List of Publication

1. R. Katiyar, V. Gupta, and R.B. Pachori, "FBSE-EWT based approach for the determination of respiratory rate from PPG signals", IEEE Sensors Letters, In press, 2019.

Contents

List of Figures

List of Tables

List of Abbreviations

HR	Heart rate
Spo2	Blood oxygen saturation
PPG	Photoplethysmography
DSP	Digital signal processing
RR	Respiratory rate
FBSE	Fourier-Bessel series expansion
EWT	Empirical wavelet transform
EMD	Empirical mode decomposition
IMF	Intrinsic mode function
PCA	Principal component analysis
FT	Fourier transform
ECG	Electrocardiogram
RMSE	Root mean square error
CSD	Correntropy spectral density
PSD	Power spectral density
PD	Photo diode
LED	Light emitting diode
FFT	Fast Fourier transform
PCC	Pearson correlation coefficient
TVAR	Time-varying autoregressive
EEG	Electroencephalogram
WVD	Wigner-Ville distribution
AC	Alternating current
DC	Direct current

Chapter 1

Introduction

A pulse oximeter is an optical medical device allowing the noninvasive monitoring of cardiopulmonary parameters. In clinical and home care applications, this is easy to use device, usually in the form of a fingertip clip, has been widely used to acquire and display heart rate (HR), respiratory rate (RR), and arterial blood oxygen saturation (SpO2) [4]. When the pulsatile waveform, such as photoplethysmogram (PPG) [5,6], yielded by one excitation wavelength in the pulse oximeter [7,8] sensor is further interpreted, many other physiological parameters can be derived. The PPG records change in blood volume over a certain length of vascular tissue, and this volumetric signal is driven by the blood pressure waveform and also constrained by the compliance of the vascular walls. Hence, intuitively there exists a strong correlation between the photoplethysmographic waveform and the blood pressure waveform and correlation has been addressed in the literature [9–11]. A PPG can be considered as a series of continuous snapshots of the circulatory system with respect to blood volume, and the character of these snapshots is determined by the measurement site of the pulse oximeter. Hemodynamics (the study of the circulation [12], including cardiac hemodynamics [13] and arterial hemodynamics [14]) guide the physiological and mathematical relationship between blood flow, blood velocity, blood pressure, blood volume, and other cardiac and arterial characteristics [15–17]. Due to its non-invasive nature, pulse oximetry is a popular technique of patient monitoring. The comprehensive physiological data that is accessible through its use is another advantage of this model. While measurements of arterial oxygen saturation (SpO2) [18] and cardiac HR are typically carried out by pulse oximeter, the information on HR and RR [19] can also be taken from sensor data. This provides a major benefit in remote patient surveillance, because wearable surveillance systems are smaller for portability and field use by delivering all physiological measurements on a single sensor [20, 21]. In particular, measurements of SpO2, HR, and RR have been investigated since critical patient data has known during medical diagnoses [22, 23].

Much efforts have been devoted over the last few years towards developing efficient algorithms for determining RR and HR from PPG signals. The scope of this thesis is to examine the potential of using Fourier-Bessel series expansion (FBSE) based empirical wavelet transform (EWT) (FBSE-EWT) for extraction of RR and HR. This chapter provides a brief introduction to the PPG signal, circuit, and an overview of the literature on existing methods for determining HR and RR from PPG signals.

1.1 Photoplethysmography (PPG)

PPG is a method of applying a light source and a light sensor on the opposite or on the same side of peripheral body parts such as finger (Fig. 1.2), ear lobe, or toe [24], for measuring the alterations in light intensity that passes through the tissue [25]. The alterations in light intensity are mainly due to the change in the volume of the absorbing materials and due to the scattering effects of light. It is a low cost, simple, portable, and non-invasive technology [26, 27], usually used for measuring percent oxygen saturation, blood pressure, and cardiac output, and to understand autonomic nervous system function, and peripheral vascular disease in clinical settings. If the light source and the sensor are both placed on the same side of the body part, then the type of probe is called a reflectance probe [28], while if they are placed on opposite sides then it is called a transmittance probe. Reflectance probe measures the intensity of light reflected by the tissue sample, while transmittance probe measures the attenuation of incident light intensity after its passes through the sample. The interaction of light with tissue sample is explained by several optical processes such as scattering, absorption, reflection, transmission and florescence [29, 30]. The attenuation of light is mainly caused by changes in blood volume and in the orientation of blood vessels [31], and it's wall movement. Thus, a typical PPG signal is related to the study of the circulation of blood through the body parts. The light absorption of tissue elements is shown in the Fig. 1.1. This signal comprises of two main components: alternating current (AC) and direct current (DC). AC is the pulsatile component as detected by the light sensor, pertaining to the synchronous changes in the blood volume with each heart beat. DC component, on the other hand, is related to the slowly changing baseline depending on respiration, sympathetic nervous system activity and thermoregulation [29]. In Fig. 1.2, we have shown the operations of PPG sensors for finger application.

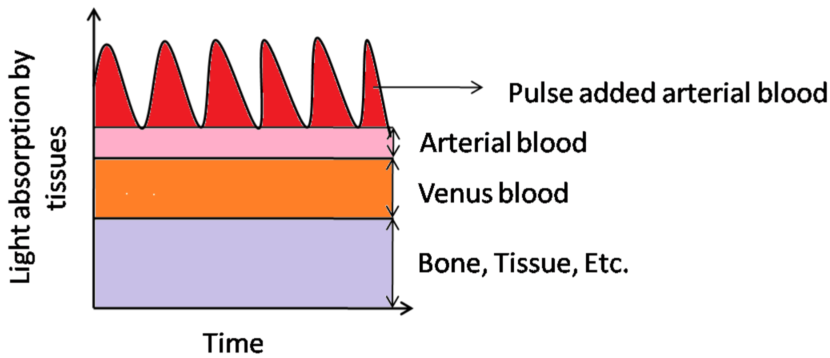

Figure 1.1: Absorption of light by tissue components [1].

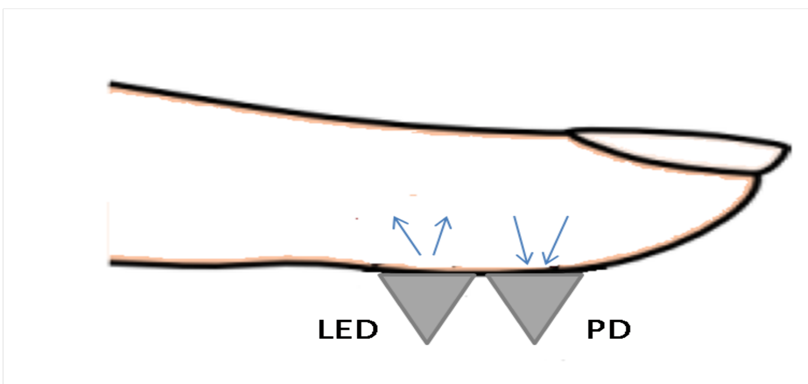

Figure 1.2: Light transmitted into the finger is reflected back and detected by a photo diode [2].

1.2 SpO2 Measurement

Injuries in an accident often impact the heart and lung of a patient immediately and often lead to blood loss, hemothorax, pneumonothea and other hazardous illnesses conditions [32]. SpO2 measurements are used regularly to identify such hypoxic occurrences before tissues and organs suffer irreversible harm.

1.2.1 HR Measurement

HR is an essential measurement during any type of trauma assessment as it estimates patient's current stability. Therefore, this kind of measurement is extremely essential for a fighting medic to quickly evaluate the stability of the victim [32–34].

If the heart contracts during systole, the systemic circulation forces extra blood bolus. These regular blood volume distortions bring pulsating components into the PPG signal. Individual pulses are the same as heart contractions, with favorable peaks in systoles and adverse peaks at the end of diastolic times. The frequency of the pulsative element should also be observed as the frequency corresponds to the HR of the subject.

1.2.2 RR Measurement

The RR is an essential measurement for diagnosis. Substantially increased or decreased RR values may show impending damage changes in a person's status during injury or trauma [32]. Thus, before arrival at a medical facility, these measurements have been identified as a helpful triage instrument and are essential to medical staff [35].

There are presently many techniques to monitor a subject's RR. In most cases, direct airflow through the mouth or nasal passage or chest or abdomen expansion is measured because of respiratory stress [36, 37]. The devices that are typically used for these measures are thermistors and pressure transducers. It can measure variation in thoracic impedance, resistive slashes, and pressure bulbs in order to record the development in the chest or abdomen by means of oral and nasal airflows. These respiratory activity surveillance techniques are unfit for application in a hostile combat setting since mild concentrations of activity can impact its precision. Moreover, the equipment used is often unmanageable and patients can prevent them from doing ordinary operations. The function of the pulmonary system affects cardiovascular flow and blood volume directly. Consequently, respiratory activities affect the PPG signal. The complexity of the cardio-pulmonary interactions means that the PPG waveforms have been modified several times [38].

1.3 Basic circuit for PPG recording

For acquisition of the PPG signal the signal must be collected from the patient's body. Therefore the PPG signal is necessary for use on the instruments so as to prevent the movement artifacts as much as possible. The noise has a significant influence on quality and readability of the PPG signal because it shows small amplitudes, i.e. the environment, the condition of a patient, respiration or motion cause multiple noises in the PPG signals. Every noise form includes a number of different frequencies [39, 40]. For example, the range of frequencies for HR and RR are 0.75-2.5 Hz and 0.05–0.75 Hz, respectively and the frequency of movement artifacts induced by movement of patient is 0.1 Hz. The PPG sensor is made up simply with a light emitting diode (LED) and a phototransistor receiver. Filtering and amplification circuits are also to be used for the assessment of this signal. In [41], the signal in the phototransistor is filtered with a low pass filter to eliminate high frequency noise. In addition, the DC monitoring technique was used to remove the DC component of the signal. After that [42, 43], another low pass filter used to remove the DC component and the artifacts. This signal will then be subtracted from the original signal and amplified by amplifier. Finally, an operational amplifier is used to amplify gain [44–47]. We have shown basic circuit implementation in flow chart in Fig.1.3.

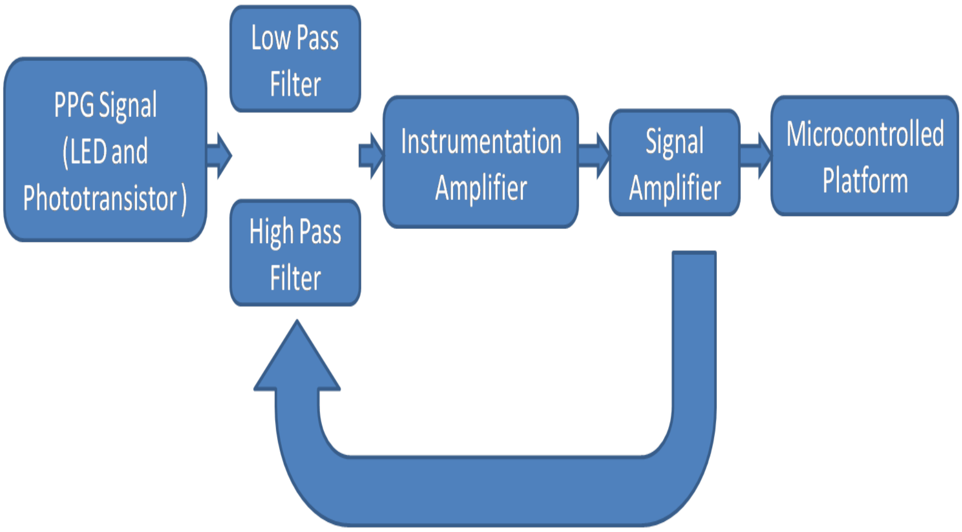

Figure 1.3: PPG instrumentation [3].

1.4 Overview of the existing techniques for extraction of RR and HR from PPG signals

Nakajima et al. [48, 49], suggested extraction of RR from PPG signal using simple band pass filter. Some researchers have done RR and HR estimation by dominant frequency using spectral analysis, which are as follows:

- Fast Fourier Transform (FFT) based method [28, 50, 51].
- Yule–Walker algorithms based approach [52, 53].
- The Welch periodogram based technique [54, 55].
- The short-time Fourier transform based method [56, 57].
- The Lomb–Scargle periodogram based approach [58, 59].
- Sparse signal reconstruction based technique [60, 61].

Some other methods have been described below to estimate dominant frequency. Addison et al. [62, 63] calculated respiratory frequency of a scalogram using the continuous wavelet transform. Shephali et al. [64–66] has used weighted multi signal oscillator based least-mean-square algorithm to calculate respiratory frequency. In [67, 68], authors used adaptive notch filter to calculate instantaneous RR. Mirmohamadsadeghi et al. [69,70] used an adaptive band pass filter to estimate instantaneous RR and HR. In [71–73], authors used a bank of notch filters to calculate HR and RR for a single signal or multiple signals. Another method to calculate dominant frequency is autoregressive all-pole modeling i.e. either the highest magnitude pole [74], or the lowest frequency pole [75–77].

Extraction of respiratory and heart information from PPG signal is actually encouraged by the work of many researchers. In [78–80], the authors proposed a secondary level feature decoupling based method to RR and HR. In their study, the authors used 12 subjects to validate their method. In [65, 78, 81], authors used the time-frequency domain based approach for RR and HR estimation of healthy subjects. In [82–84], authors used empirical mode decomposition (EMD) but this method was semi-automatic and this method requires manual selection of intrinsic mode function (IMF). Mode-mixing [85] is a limitation of the EMD method. In [86], authors used multi scale principal component analysis (MSPCA) and they have used less subject. MSPCA is a complex method to extract RR and HR from PPG signals. Nilsson et al. [87], have used band pass filter but they explained that the results are not good because of movements. In another work, Karlen et al. [88] have been proposed a method which is very sensitive for noise and the amplitude of the PPG signals can be easily corrupted by noise. In [85, 89], authors have applied ensemble EMD with principal component analysis (PCA) (EEMD-PCA) on PPG signals. The obtained IMFs in this method have information about the RR and HR. After that, they have used PCA for the selection of significant IMFs. These proposed works have been delivered significant contributions to the literature.

However, these methods have certain limitations such as involvement of less number of subjects, mode-mixing problems, and high computational complexity. Hence, we have formulated a new method to overcome the limitations of the previous works.

1.5 Motivation

PPG signal is very prone to noise. The most challenging part is to measure the HR and RR from PPG signals as they are corrupted by motion artifacts. In case of sleep studies, using optical devices is not a serious problem, but it becomes difficult if the devices worn during exercise. The sensitivity of the signal decreases because of the motion between sensor and skin. We can minimize the impact by making the device attachment to the body more tightly, but not completely. Therefore, PPG signals become noisy in recording time. Several methods have been developed as a result of these research efforts. Various non-stationary signal analysis methods have been used to estimate HR and RR from PPG signals [65,78,82,83,85]. In the existing techniques, authors used various techniques to decompose signals and applied PCA to calculate RR and HR from PPG signals. Therefore, existing techniques are computationally complex. In [65,78], authors used the time-frequency domain based approach for RR and HR estimation of healthy subjects. EMD method was semi-automatic and this method requires manual selection of IMF. In another work, Karlen et al. [88] has been proposed a method which is very sensitive for noise and the amplitude. In [85], authors have applied EEMD-PCA on PPG signals. Hence, the motivation here is to develop such methods, which reduce noise and computational complexity to extract RR and HR from PPG signals.

1.6 Contributions of the thesis

The major contributions of the work presented in the thesis is described below. FBSE-EWT based approach is suggested to decompose PPG signals into sub-bands. In the proposed FBSE-EWT method, Bessel functions are non-stationary in nature and has been used as basis set. Therefore, this approach is appropriate for assessment of non-stationary signals like PPG signals. In the proposed method, Gaussian filter [90,91] is used to reduce noise from FBSE spectrum. Therefore, the proposed approach has provided less noisy FBSE spectrum. In the proposed technique, we have divided databases in the length of 30 seconds. We have compared results of proposed method with existing techniques. The proposed approach has provided better performance in terms of root mean square error (RMSE), box Whishker's plot, Pearson's plot, and Bland-Altmon plot.

1.7 Organization of thesis

The rest of the thesis is organized as follows:

Chapter 2 presents the detailed description of frequency spectrum using FBSE, boundary detection using scale-space method, EWT, and FBSE-EWT method.

Chapter 3 presents databases and the proposed methodology for RR and HR extraction using FBSE-EWT method.

Chapter 4 presents results and discussions section. In which,we have presented results of proposed method and comparison of these results with existing methods.

Chapter 5 presents conclusion of whole work. The directions of future research work are also provided in this chapter.

1.8 Summary

In this chapter, we have discussed about PPG signals in detail. Spo2, RR, and HR measurements have been discussed. PPG signal comprises two components. AC component shows the behaviour of HR. DC component shows the behavior of RR. A PPG can be considered as a series of continuous snapshots of the circulatory system with respect to blood volume, and the character of these snapshots is determined by the measurement site of the pulse oximeter. We have discussed EMD, EMD-PCA and other existing techniques to extract RR and HR from PPG signals. Existing methods used PCA for the selection of significant IMFs. Our goal is to reduce computational complexity and reduce noise from PPG signals.

Chapter 2

FBSE, Scale Space, EWT, and FBSE-EWT

2.1 Introduction

In this chapter, we have discussed about FBSE, scale space, Otsu's method, and EWT. We have used scale-space based boundary detection method which works on the concept of local minima. In scale space method, two local minima have been used to define a meaningful mode that leads to two long scale-space curves whose length is greater than a threshold. Threshold value has been determined by Otsu's method. The FFT spectrum has been replaced with FBSE spectrum for the estimation of optimal boundary frequencies and improved wavelet based filter bank has been obtained. The Littlewood–Paley and Meyer's wavelets have been used to design EWT filters. FBSE uses Bessel functions as basis functions, which are damped in nature, this makes FBSE suitable for non-stationary signal analysis. In Otsu's method, the selection of threshold value has been performed based on minimization of within-class variance corresponding to two groups of pixels which are separated by the thresholding operation.

2.2 FBSE

Many researches have been carried with FBSE method, few of them are discussed below.

In [92], authors discussed signal processing based on Fourier-Bessel series expansion. In many situations, representing any signal in terms of samples and predefined function is not desirable. For example, when parameters of interest are more compact in frequency domain, a signal may be determined by time domain sample values. Many practical signals are very redundant, for those signals less number of samples can be used for low bandwidth. For that purpose different transforms can be used such as FFT and FBSE.

In [93], authors have been proposed a second-order linear time-varying autoregressive (TVAR) method for electroencephalogram (EEG) parametric representation. The FBSE coefficients have been used to form a feature vector for EEG signal segmentation. They found a straightforward model for the parametric representation of the EEG signals by choosing a appropriate data length. This work has presented the full technique for estimating model parameters.

In [94], authors have overcome the problem of amplitude and frequency modulation while analyzing multi component signals, which introduce error while estimation of the modulation functions. They have used FBSE based discrete energy separation algorithm for component separation, which lead to accurate estimation of amplitude envelope and instantaneous frequency for multi component signals.

In [95], a new method has been introduced for time-frequency representation of the signal, which combines the FBSE with the Wigner–Ville distribution (WVD). Applying WVD directly to a multi component signal leads to cross terms. The FBSE decomposes a multi component signal and then, WVD method is applied to components of the signal for analyzing the time-frequency distribution.

Therefore, FBSE-EWT has been used in this work for PPG decomposition. FBSE technique has been discussed below in detail.

i) Obtain the spectrum using FBSE method: The FBSE-EWT [96] has been applied in order to obtain sub-bands of PPG signal. In FBSE, the number of coefficients for spectral representation equal to the length of the discrete signal, whereas spectrum length is half of the discrete signal in Fourier representation [94, 97–99]. Thus, the frequency resolution is double for FBSE as compared to Fourier transform. The FBSE-EWT method also requires less computational complexity than EEMD-PCA method [85]. FBSE-EWT method has been used to decompose PPG signal $x(t)$ into N sub-bands as follows: i) Obtain the spectrum using FBSE method: Using zero-order Bessel functions, the FBSE of $x(t)$ is expressed in the following mathematically as [92, 100–102]:

$$x(t) = \sum_{i=1}^{H} C_i J_0\left(\frac{\beta_i t}{H}\right), t = 0, 1, ..., H - 1 \tag{2.1}$$

where, C_i are known as the FBSE coefficients of $x(t)$ which can be expressed as follows [102–105]:

$$C_i = \frac{2}{H^2 (J_1(\beta_i))^2} \sum_{t=0}^{H-1} t x(t) J_0\left(\frac{\beta_i t}{H}\right) \tag{2.2}$$

where, the $J_0(.)$ and $J_1(.)$ functions denote the zero and first order Bessel functions, respectively. The ascending order positive roots corresponding to zero-order Bessel function ($J_0(\beta) = 0$) are represented by β_i with $i = 1, 2, ..., H$. Here, order i is corresponding to continuous-time frequency f_i (Hz) with the peak value as [92, 106, 107]:

$$\beta_i \approx \frac{2\pi f_i H}{f_s} \tag{2.3}$$

where $\beta_i \approx \beta_{i-1} + \pi \approx i\pi$, f_s denotes the sampling frequency, and this expression can be written as [92, 108–110]:

$$i \approx \frac{2 f_i H}{f_s} \tag{2.4}$$

Here, i should vary from 1 to H for covering the whole bandwidth of $x(t)$.

2.3 Scale space

In [111], authors has detected boundaries in Fourier spectrum by finding local maxima but in real time signal, Fourier support has failed to detect accurate boundaries.

Authors have normalized the spectrum between 0 to π. Then, they have calculated all the local maxima and detected boundary in between them. This task is effective when spectrum consists distinct modes. The problem in this method [112] is, it detects boundary equidistance to two successive maxima. An easy way of avoiding this scenario is by keeping the lowest minima in that segment.

When we look at the spectrum profile of a signal in which a lot of energy is concentrated with lots of local maxima but in the same mode. To eliminate this situation, the logarithm must be used to remove the global trend of the analyzed spectrum before the detection task. This method is called global trend removing [112]. In this section, scale space method has been discussed in detail.

Witkin [113] and Koenderink's [114] methodologies for obtaining a multi-scale representation is by inserting an original signal into a family of derived signals. The parameter m denotes the scale parameter, which describes the current scale level.

For a discrete signal $x(n)$, the scale-space representation can be achieved by evaluating the $x(n)$ convolution with Gaussian kernel, which can be mathematically expressed as [115–117]:

$$\delta(h,m) = \sum_{n=-P}^{P} x(h-n)z(n;m) \tag{2.5}$$

where, $z(n;t) = \frac{1}{\sqrt{2\pi m}} e^{\frac{-n^2}{2m}}$, $P = K\sqrt{m}+1$ with $3 \leqslant K \leqslant 6$, and m is a scale parameter. Here, the number of minima in the scale-space plane reduces if the scale parameter ($\gamma = \sqrt{\frac{m}{m_0}}, \gamma = 1, 2, \ldots \gamma_{\text{maximum}}$) rises, and no new minima will be appeared. Let N_0 is the total number of initial minima then for each initial minima G_i produces a curve K_i of length B_i in the scale-space plane. Here, the value of i varies from 1 to N_0. The length (integer) B_i can be mathematically expressed as [118–120]:

$$B_i = \text{maximum}\left\{\frac{\gamma}{\text{the } i^{\text{th}} \text{ minimum exists}}\right\} \tag{2.6}$$

The meaningful modes using this concept can be defined in the histogram as follows: Two local minima have been used to define a meaningful mode that leads to two long scale-space curves K_i whose length is greater than a threshold T. Thus, the optimal value of T is required in order to obtain the scale-space curves with a length higher than the T. The Otsu's [121,122] technique has been utilized here for the determination of T and meaningful modes have been extracted. In Otsu's method [121,123], the selection of T has been performed based on minimization of within-class variance corresponding to two groups of pixels which are separated by the thresholding operation.

2.3.1 Otsu's method

Otsu's method [121,123] is described as follows:

Variance is a measure of region's homogeneity (i.e. low variance between areas with low uniformity). Otsu's technique chooses the threshold by minimizing the within-class variance of the two groups of pixels, which is separated by the thresholding operator. In next section, we have discussed in detail to determine the threshold value. In this method, mean and variance have been used to find threshold value.

Means and variances

Consider the histogram with a gray level L (i.e. Pi is a standardized frequency of i for each gray level value). If the threshold has been set to T, the usual fraction of pixels to be classified as a background and object can be given as follows [121,123]:

$$\begin{aligned} q_b(T) &= \sum_{i=1}^{T} P_i \\ q_0(T) &= \sum_{i=T+1}^{L} P_i \end{aligned} \tag{2.7}$$

where, $q_b(T) + q_0(T) = 1$. The gray mean value of background and object pixels is expressed as follows [121,124,125]:

$$\begin{aligned} \mu_b(T) &= \frac{\sum_{i=1}^{T} iP_i}{\sum_{i=1}^{T} P_i} = \frac{1}{q_b(T)} \sum_{i=1}^{T} iP_i \\ \mu_0(T) &= \frac{\sum_{i=1+T}^{L} iP_i}{\sum_{i=1+T}^{L} P_i} = \frac{1}{q_0(T)} \sum_{i=1+T}^{L} iP_i \end{aligned} \tag{2.8}$$

The mean gray-level value over the whole image (grand mean) is expressed as follows [121, 126, 127]:

$$\mu = \frac{\sum_{i=1}^{L} iP_i}{\sum_{i=1}^{L} P_i} = \sum_{i=1}^{L} iP_i \tag{2.9}$$

In the whole image, the mean value in gray level is expressed as follows [121, 123, 128]:

$$\begin{aligned} \sigma_b(T)^2 &= \frac{\sum_{i=1}^{T}(i-\mu_b)^2 P_i}{\sum_{i=1}^{T} P_i} = \frac{1}{q_b(T)} \sum_{i=1}^{T}(i-\mu_b)^2 P_i \\ \sigma_0(T)^2 &= \frac{\sum_{i=1+T}^{L}(i-\mu_0)^2 P_i}{\sum_{i=1+T}^{L} P_i} = \frac{1}{q_0(T)} \sum_{i=1+T}^{L}(i-\mu_0)^2 P_i \end{aligned} \tag{2.10}$$

The variance of the entire image is expressed as follows [121, 129, 130]:

$$\sigma^2 = \sum_{i=1}^{L}(i-\mu)^2 P_i \tag{2.11}$$

Within-class variance and between-class variance

The variance σ can be expressed as follows [121, 123, 131]:

$$\begin{aligned} \sigma^2 &= q_b(T)\sigma_b(T)^2 + q_0(T)\sigma_0(T)^2 + q_b(T)(\mu_b(T)-\mu)^2 + q_0(T)(\mu_0(T)-\mu)^2 \\ &= \sigma_W(T)^2 + \sigma_B(T)^2 \end{aligned} \tag{2.12}$$

where, $\sigma_W(T)^2$ and $\sigma_B(T)^2$ has been specified as within-class variance and between-class variance, respectively.

Determining the threshold

As σ does not rely in its complete variability on T, the T that minimizes $\sigma_W(T)^2$ will be T that maximizes $\sigma_B(T)^2$ $\sigma_B(T)^2$ can be rewritten as follows [121, 132]:

$$\sigma_B{}^2 = \frac{[\mu(T) - \mu q_B(T)]^2}{q_B(T) q_0(T)} \tag{2.13}$$

where $\mu_T = \sum_{i=1}^{T} iP_i$ and that maximizes $\sigma_B{}^2$ will be the threshold T.

2.4 Empirical wavelet transform

EWT is a process of signal decomposition with adaptiveness in the process by using modes. EWT [111] is developed by the Jerome Gilles in 1998 motivated from EMD proposed by Huang et al. [133]. The process of the EWT is performed in the following way:

1. The frequency components of the signal are computed using Fourier transform (FT).

2. The Spectrum is segmented into N continuous segments centred around W_n by assuming Fourier spectrum in $[0, \pi]$.

3. The wavelet and scaling function are related to every segment in the form of band pass filter functions. The segmentation provides the scheme flexibility as per the signal analysis.

For each obtained segment, the wavelet and empirical scaling functions have been designed as band pass filters. The Littlewood–Paley and Meyer's wavelets have been used to design these filters [111, 120, 134, 135]. The mathematical expressions of empirical scaling and wavelet functions in frequency domain are as follows [111, 136, 137]:

$$\lambda_i(W) = \begin{cases} 1 & ,\text{if } |W| \leq (1-\mu)W_i. \\ \cos\left[\frac{\pi\sigma(\mu,W_i)}{2}\right] & ,\text{if } (1-\mu)W_i \leq |W| \leq (1+\mu)W_i. \\ 0 & ,\text{otherwise.} \end{cases} \tag{2.14}$$

$$\vartheta_i(W) = \begin{cases} 1 & ,\text{if } (1+\mu)W_i \leq |W| \leq (1-\mu)W_{i+1}. \\ \cos\left[\frac{\pi\sigma(\mu,W_{i+1})}{2}\right] & ,\text{if } (1-\mu)W_{i+1} \leq |W| \leq (1+\mu)W_{i+1}. \\ \sin\left[\frac{\pi\sigma(\mu,W_i)}{2}\right] & ,\text{if } (1-\mu)W_i \leq |W| \leq (1+\mu)W_i. \\ 0 & ,\text{otherwise} \end{cases} \tag{2.15}$$

Where $\sigma(\mu, W_i) = \phi\left[\frac{(|W|-(1-\mu)W_i)}{2\mu W_i}\right]$ and $\phi(n)$ is an arbitrary function defined as [111, 138–140],

$$\phi(n) = \begin{cases} 0 & ,\text{if } n \leq 0. \\ \phi(n) + \phi(1-n), \forall\ n & \in [01]. \\ 1 & ,\text{if } n \geq 1. \end{cases} \tag{2.16}$$

The condition of tight frame for μ is expressed as follows [100, 111, 141]:

$$\mu < \text{minimum}_i \left(\frac{W_{i+1} - W_i}{W_{i+1} + W_i} \right) \tag{2.17}$$

Afterward, to obtain the approximation and detail coefficients, inner product has been applied to the wavelets and scaling function with analyzed signal, which are mathematically expressed as [94, 111, 142, 143],

$$\chi_{M,\vartheta}(i,t) = \int M(\tau)\overline{\vartheta_i(\tau - t)}d\tau \tag{2.18}$$

$$\chi_{M,\lambda}(0,t) = \int M(\tau)\overline{\lambda_1(\tau - t)}d\tau \tag{2.19}$$

Where, the detail coefficients are represented as $\chi_{M,\vartheta}(i,t)$ for i^{th} oscillatory level and approximation coefficients are represented as $\chi_{M,\lambda}(0,t)$. Finally, the reconstruction of these sub-band signals can be expressed as follows [111, 134, 144]:

$$f_0(t) = \chi_{M,\lambda}(0,t) * \lambda_1(t) \tag{2.20}$$

$$f_i(t) = \chi_{M,\vartheta}(i,t) * \vartheta_i(t) \tag{2.21}$$

Where, symbol $(*)$ represents convolution operation. In equations 2.20 and 2.21, approximate sub-band signal represented as $f_0(t)$ and detail sub-band signal represented as $f_i(t)$ of i^{th} level.

2.5 FBSE-EWT method

In the proposed method, The FBSE is used in order to obtain the frequency spectrum of the analyzed signal. The FFT based spectrum is not used in the EWT method for the boundary detection and spectrum segmentation purpose. FBSE coefficients are useful for the spectral analysis of non-stationary signals because of the nonstationary nature of Bessel functions. It has been observed that FBSE spectrum has compact representation as compared to conventional Fourier representation and avoids windowing for spectral representation. Thereafter, scale-space based boundary detection approach was applied to find meaningful modes based on that we have found boundaries and to segment the FBSE spectrum which result in improved EWT based filter bank and sub-band signals are obtained. The mechanism of EWT is based on the formation of adaptive wavelet-based filters. The wavelet-based filters provide support to the spectrum information location of the analysed signal. FBSE-EWT method has been depicted in Fig. 2.1.

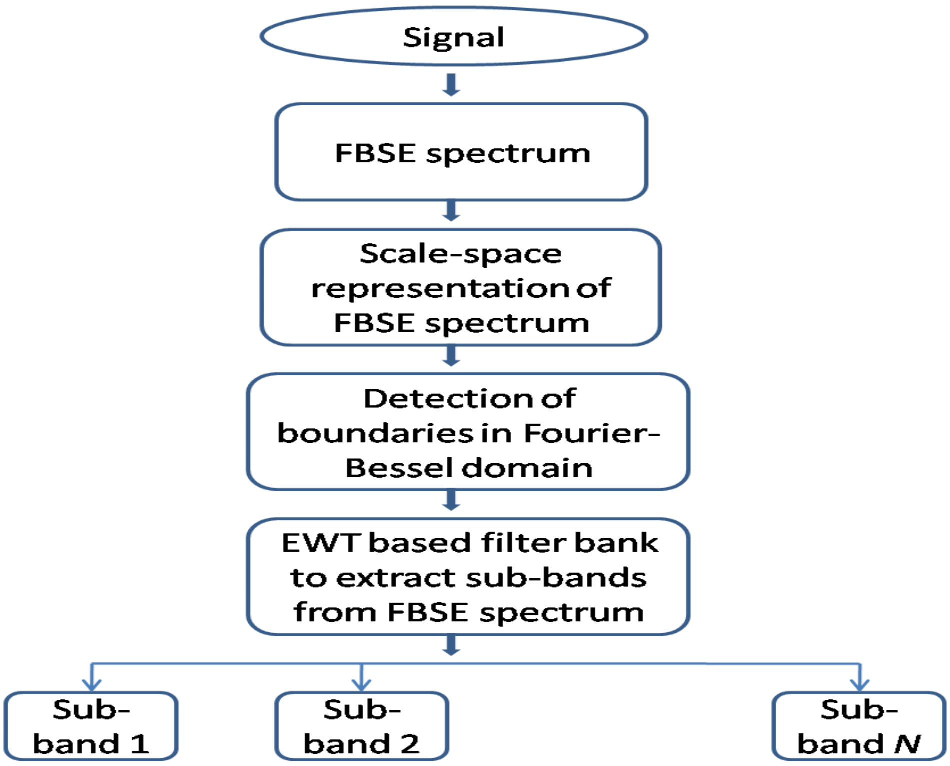

Figure 2.1: FBSE-EWT method.

2.6 Summary

In this chapter, FBSE, scale-space, Otsu's method, and EWT have been discussed briefly. In FBSE method, Bessel functions have been used as bases. Because of Bessel's non-stationary nature, FBSE coefficients are helpful for the spectral assessment of non-stationary signals. In FBSE, the number of coefficients for spectral representation equal to the length of the discrete signal, whereas spectrum length is half of the discrete signal in Fourier representation [100, 145]. Thus, the frequency resolution is double for FBSE as compared to FT. Scale-space method has been used for spectrum segmentation. In scale space method, two local minima have been used to define a meaningful mode that leads to two long scale-space curves whose length is greater than a threshold. Threshold value has been determined by Otsu's method. The selection of threshold value has been performed based on minimization of within-class variance corresponding to two groups of pixels which are separated by the thresholding operation. After that, EWT has been discussed. In EWT, the wavelet and empirical scaling functions have been designed as band-pass filters and the Littlewood–Paley and Meyer's wavelets have been used to design these filters.

Chapter 3

Datasets and Proposed Method

3.1 Introduction

In this chapter, we have discussed about MIMIC and capnobase databases and proposed method in detail. 310 and 632 epochs have been used from MIMIC and capnobase databases, respectively. FBSE has been used for frequency spectrum representation. Then, scale-space method has been used for boundary detection. After that, EWT based filter bank has been used for the extraction of sub-bands. In the proposed method, FBSE-EWT method has been used to extract RR and HR. Only first and second sub-bands have information about respiratory and heart activity. Using this method, we have reduced computationally complexity of existing methods. In this chapter, Whisker's plot, Pearson's plot, Bland-Altman plot and RMSE have been used for performance evaluation to compare with existing methods.

3.2 Datasets

We have used publicly available two independent datasets: MIMIC and capnobase datasets for measuring the effectiveness of the suggested approach in this method.

3.2.1 MIMIC database

The MIMIC dataset [146] is available online which consists of 72 simultaneously recorded PPG, respiratory, blood pressure, and electrocardiogram (ECG) signals. Sampling frequency for these signals is 125 Hz. In our method, we have compared RR extracted from PPG signals with reference RR derived from the respiratory signal. The main purpose of using this database is that this database has simultaneous recorded PPG and respiratory signals which help us in verifying the results. In this work, we have manually selected 310 epochs of 30 seconds duration from simultaneously recorded respiratory and PPG signals.

3.2.2 Capnobase database

The capnobase database [147], is another publicly available data set which also consists simultaneously recorded respiratory, ECG, and PPG signals. These signals are recorded from 29 children and 13 adults at the time of routine anesthesia and elective surgery in St. Paul's Hospital and British Columbia Children's Hospital, respectively [88,148]. S/5 Collect software (Datex-Ohmeda, Finland) has been used for the recording of this database and sampling frequency of these signals is 300 Hz [88]. In this work, we have used 632 epochs of 30 seconds duration obtained with simultaneously recorded respiratory and PPG signals.

3.3 Proposed method

In this chapter, we have explained our proposed a method for analysing PPG signals. The block diagram of the proposed method FBSE-EWT in order to obtain RR and HR from PPG signals has been depicted in Fig. 3.1. The analyzed signal's frequency spectrum has been obtained using FBSE technique in the proposed technique. The spectrum based on FT has not been used to detect boundaries and segment the spectrum. The FBSE coefficients are helpful for the spectral assessment of nonstationary signals due to use of Bessel functions which are nonstationary in nature. Compared with the standard Fourier representation, FBSE spectrum has been found to be compact and avoids windowing for spectral representation as compared to FT based representation. Therefore, scale-space based boundary detection approach has been applied to segment the FBSE spectrum. After that, EWT based filter bank has been used for the extraction of sub-bands. The EWT mechanism is based on the development of adaptive wavelet filters [149].

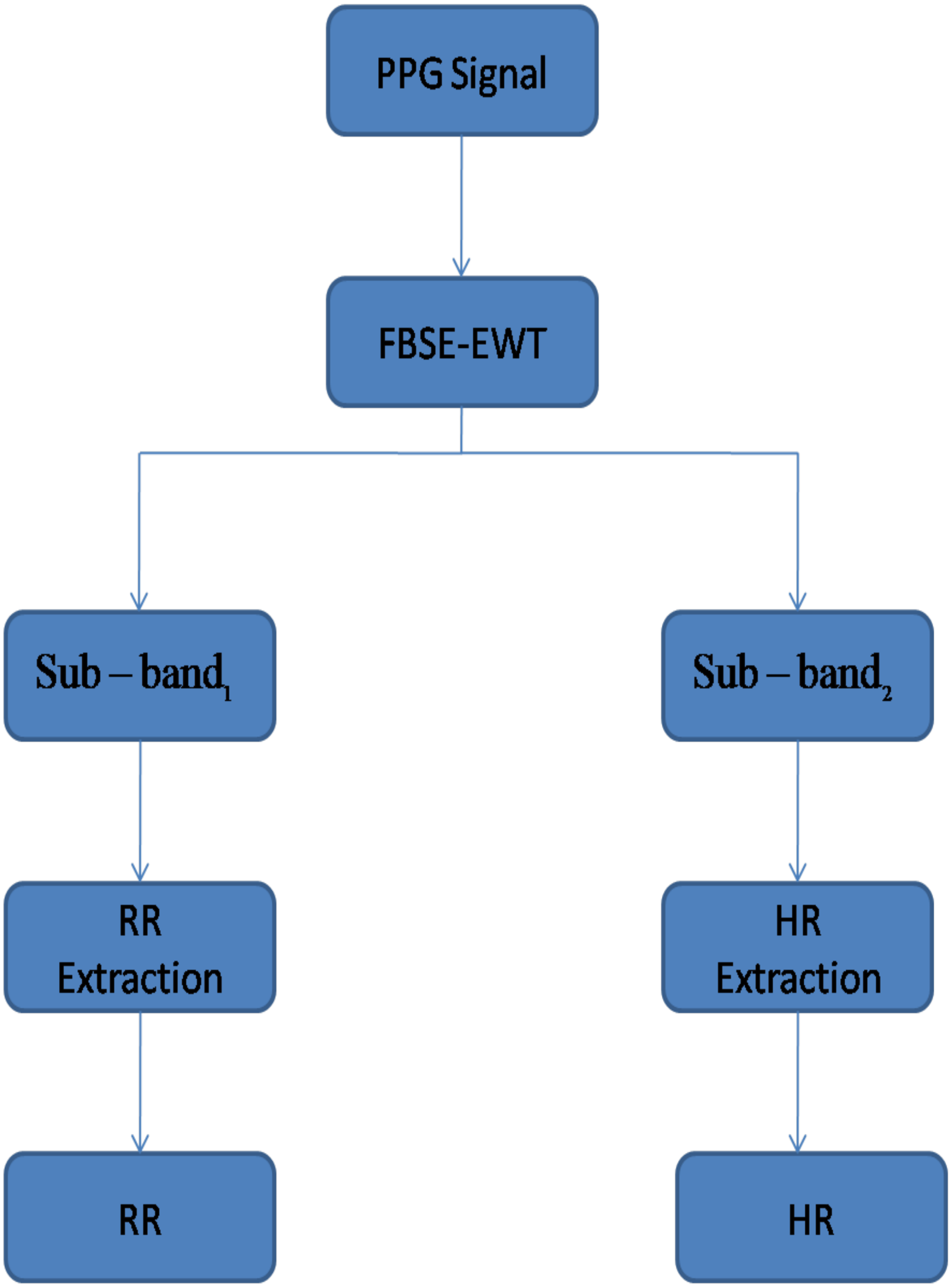

Figure 3.1: FBSE-EWT technique for extracting RR and HR from PPG Signal

3.3.1 Decomposition of PPG signal using FBSE-EWT

The FBSE-EWT [96] has been applied in order to obtain sub-bands of PPG signal. In FBSE, the number of coefficients for spectral representation equal to the length of the discrete signal, whereas spectrum length is half of the discrete signal in Fourier representation [94]. Thus, the frequency resolution is double for FBSE as compared to Fourier transform. The FBSE-EWT method also requires less computational complexity than EEMD-PCA method [85]. FBSE-EWT method has been used to decompose PPG signal $x(t)$ into N sub-bands as follows:

Step 1: Obtain the spectrum using FBSE method.

Step 2: Segmentation of FBSE spectrum.

Step 3: Obtain sub-bands.

3.3.2 Selection of first sub-band and second sub-band

For 2 to 18 years old young adults and children, the normal range of RR and HR are 8 to 45 breaths/min and 45 to 145 beats/min, respectively. In FBSE-EWT method, Gaussian filter is used for regularization purpose. This filter reduces noise from the spectrum of signal. Therefore, we have got only first sub-band and second sub-band of each epoch is within the range 0.05-0.75Hz and 0.75-2.5Hz, respectively. Hence, we have only considered first sub-band (sub-band$_1$) and second sub-band (sub-band$_2$) for further processing and other sub-bands have been rejected out.

3.3.3 Extraction of RR and HR

Since the first and second sub-bands of each epoch expressed the respiratory and cardiac information then FBSE has been utilized on the first and second sub-bands of each epoch to extract frequency (f_{RR} and f_{HR}) and then it was converted to RR and HR using following mathematical expression [89]:

$$\mathrm{RR} = f_{RR} \times 60 \text{ (breaths/min)} \tag{3.1}$$

$$\mathrm{HR} = f_{HR} \times 60 \text{ (beats/min)} \tag{3.2}$$

We have calculated reference RR and HR manually from the reference respiratory and ECG signals from MIMIC and capnobase databases. For reference RR and HR calculation, we have selected data length of 30 seconds from respiratory and ECG signals, respectively. After that, we have applied FBSE to calculate the dominant frequency, frequency at which highest peak has obtained in magnitude spectrum.

3.4 Performance evaluation

3.4.1 Pearson's correlation coefficient

The covariance of two variables P and U is defined as [150]:

$$Cov(P,U) = E(PU) - E(P)E(U) \tag{3.3}$$

We can standardize it by separating it from each variable by standard deviation. This leads to a coefficient known as the Pearson correlation coefficient (PCC). PCC is the most commonly recognized measure of dependence since the information population can be calculated by as follows [150].

$$\rho(P,U) = \frac{Cov(P,U)}{\sigma_P \sigma_U} \tag{3.4}$$

where, σ denotes standard deviation. PCC (ρ) is a linear dependency measurement between two variables P and U . The ρ coefficient ranges from $-1 \leq \rho \leq +1$.

The correlation of Pearson is significantly affected by outliers, unfair variations, normality, and linearity.

3.4.2 Box-Whisker plot

A box plot is the easy way of representing numeric groups through the five summaries of numbers, like the least observation, lower quartile (Q1), median quartile (Q2), upper quartile (Q3), and the largest observation. This plot is used for the evaluation of the information symmetry. A box Whiskers plot [151] has a central box separated by a line with two lines from the box.The size of the centralized box shows the extent of the bulk of the information while the whisker length demonstrates how long the tails are stretched. The length of the track has no specific significance; without influencing its visual effect the track can be produced quite narrow. The median sample is presented in the box as a row. The whiskers are of the same length and the amount of extreme information points is distributed equally on each part of the track, if the distribution is symmetric, then the column is broken in equal halves by the average.

3.4.3 Bland-Altman plot

The Bland-Altman plot [152, 153] (difference plot) is a graphic technique to compare two measurement methods. The difference between the two databases is compared to the averages of the two databases in that graphical method. Alternatively, if this technique is a reference, the differences may be compared to one of the two techniques.

The horizontal lines are drawn at the mean and at the contract boundaries identified as the mean plus and minus 1.96 times the normal difference.

3.4.4 Root mean square error (RMSE)

We have measured accuracy of proposed method using root mean square error. RMSE has been calculated for each subject. Equation 3.5 given below describes RMSE.

$$\text{RMSE} = \sqrt{\frac{1}{T}\sum_{b=1}^{T}[K(b) - N(b)]^2} \tag{3.5}$$

where, $K(b)$ and $N(b)$ represent the median of reference rate and estimated rate respectively for b^{th} epoch and T is the total number of epochs.

3.5 Overview of FBSE-EWT technique for extracting RR and HR from PPG signal with waveforms

We have shown FBSE-EWT base approach for extraction HR and RR from PPG signal for a epoch.

Step 1: PPG signals which have been shown in Figs. 3.2 and 3.3 for first and second epochs.

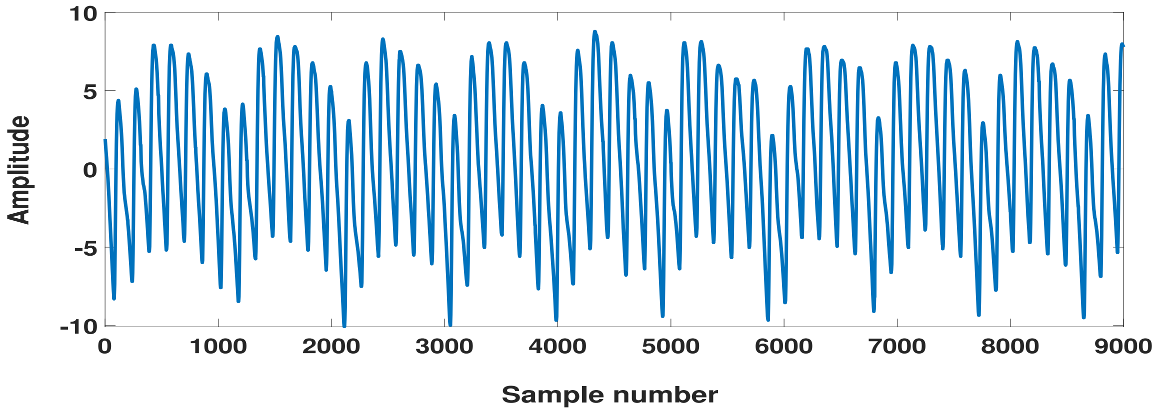

Figure 3.2: PPG signal of first epoch.

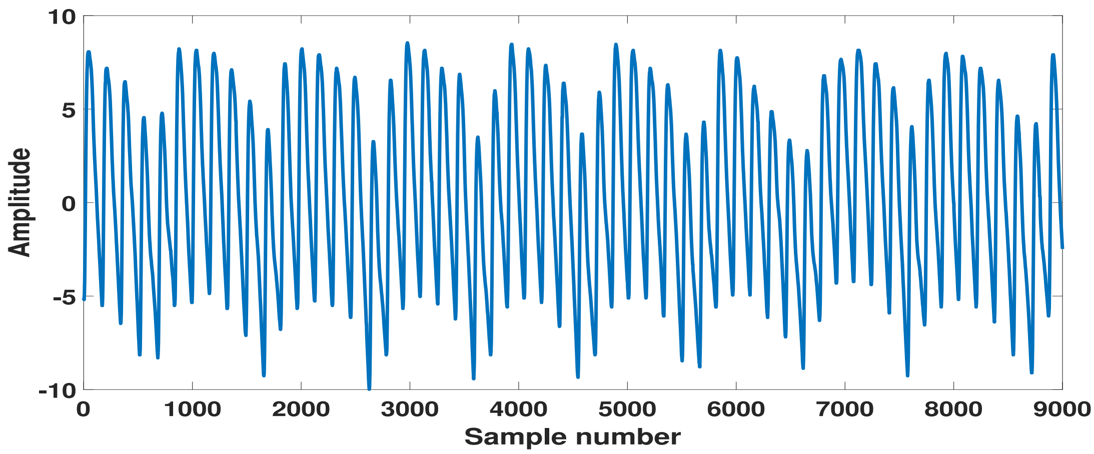

Figure 3.3: PPG signal of second epoch.

Step 2: Magnitude spectrum using FBSE and spectrum segmentation using scale-space which have been shown for both epochs in Figs. 3.4 and 3.5

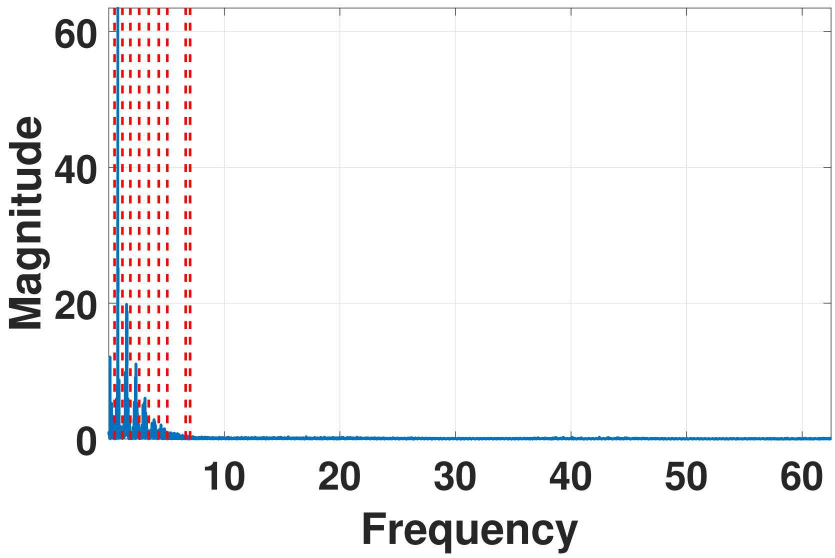

Figure 3.4: Segmented spectrum of first epoch using FBSE.

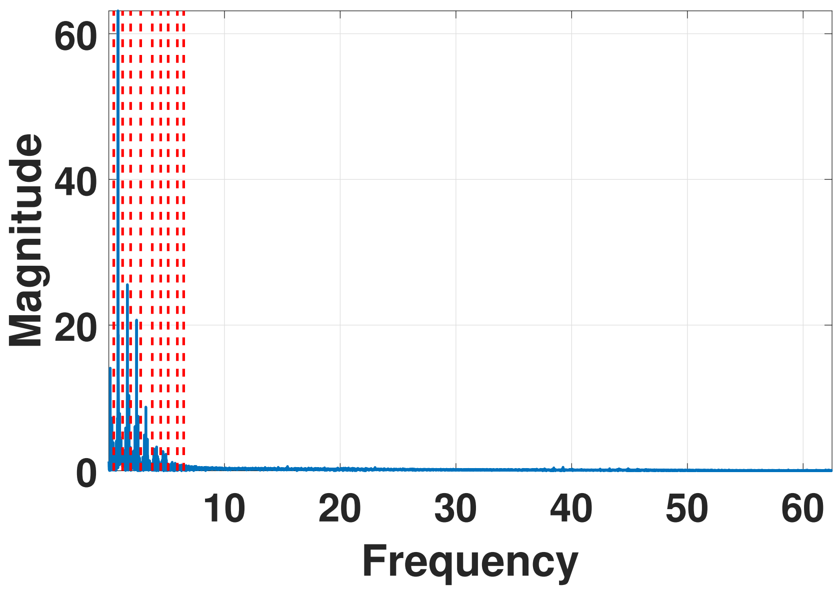

Figure 3.5: Segmented spectrum of second epoch using FBSE.

Step 3: Sub-bands of first and second epochs which have been shown in Figs. 3.6 and 3.7.

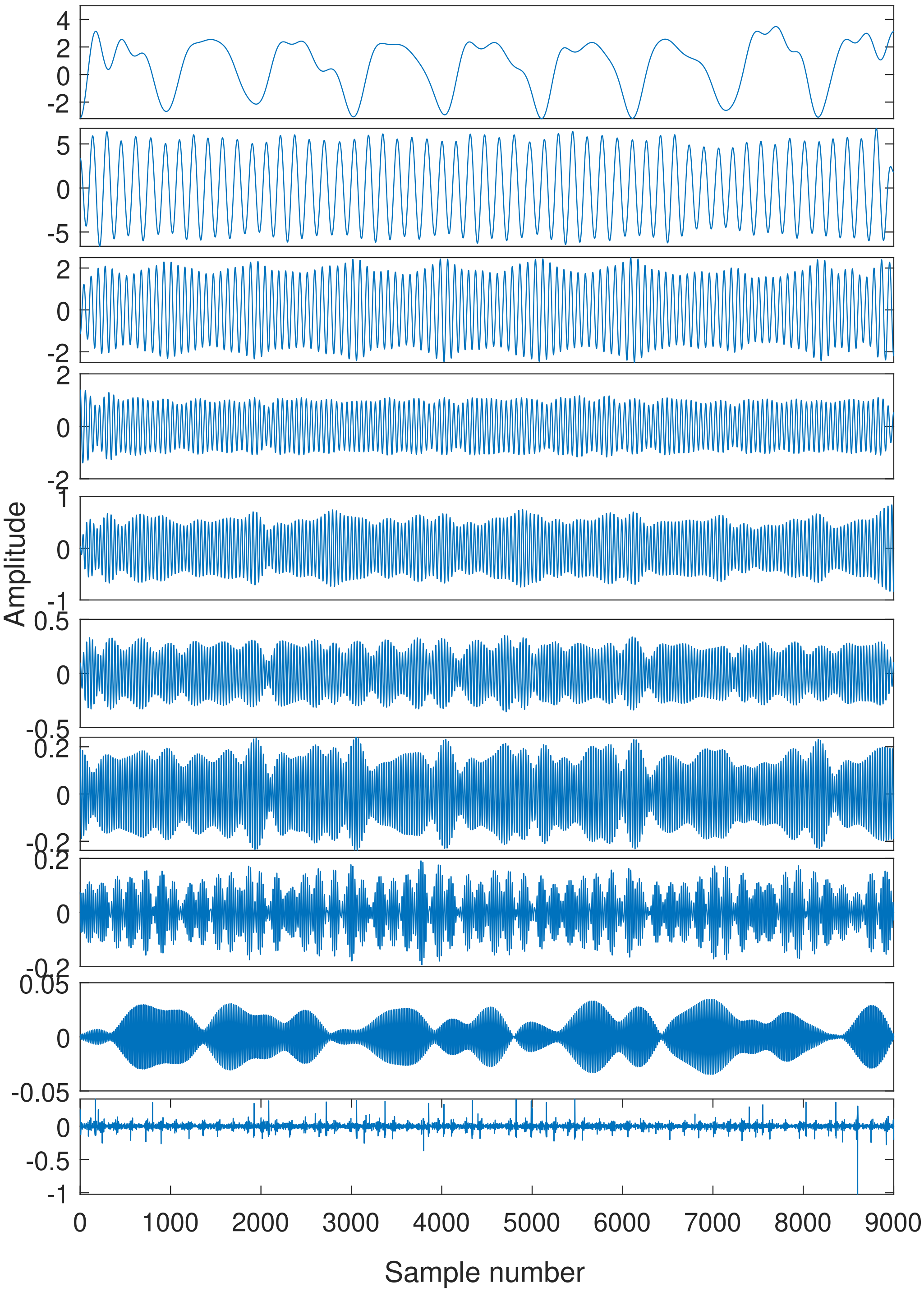

Figure 3.6: Sub-bands of first epoch.

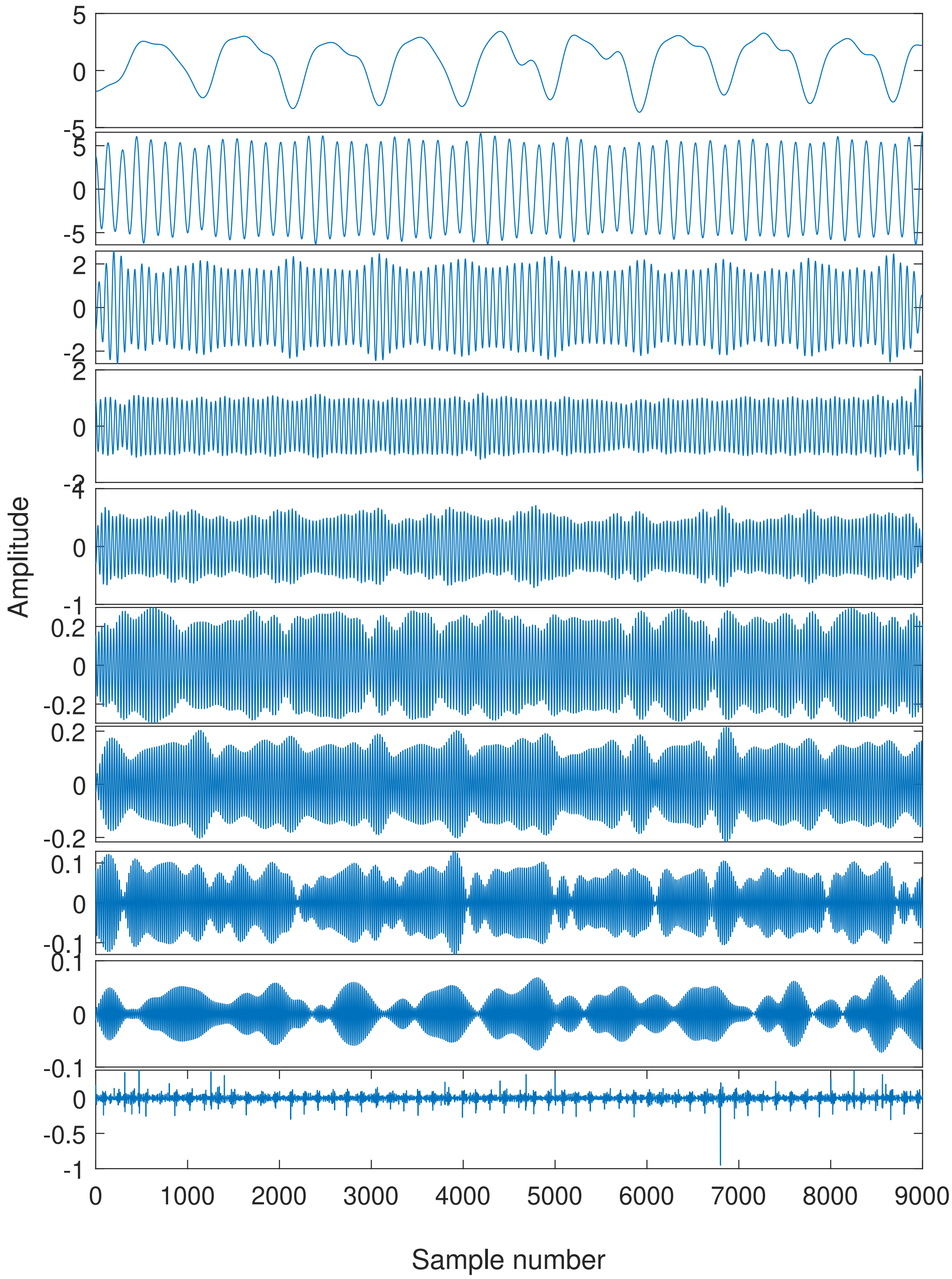

Figure 3.7: Sub-bands of second epoch.

Step 4: Extraction of sub-band1 and sub-band2 using EWT method which are shown in Figs. 3.8 and 3.9 for both epochs, respectively.

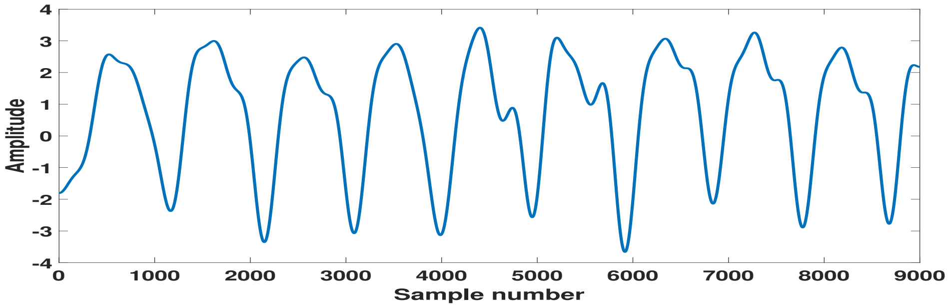

(a)

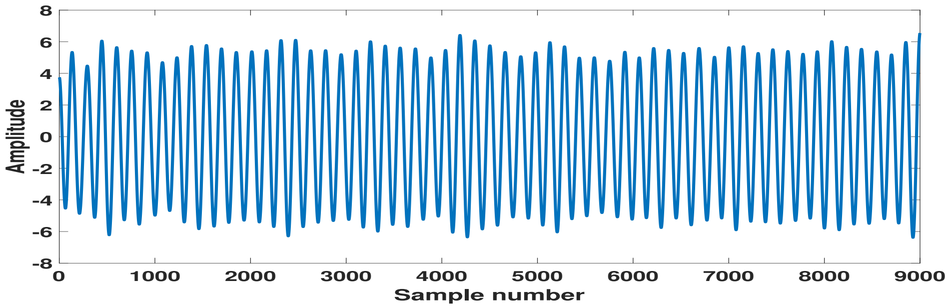

(b)

Figure 3.8: First epoch (a) Sub-band1 (b) Sub-band2.

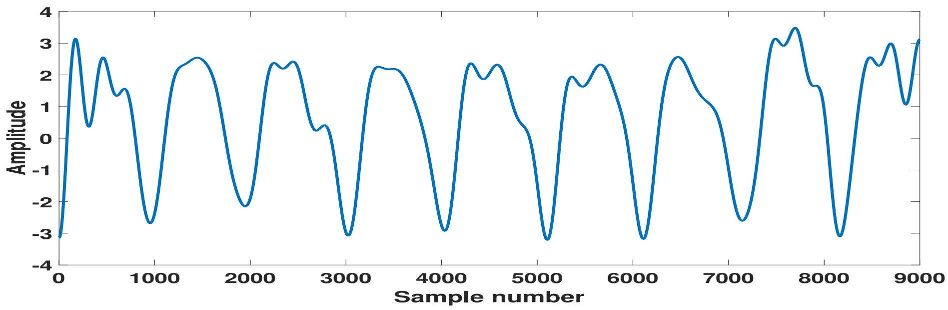

(a)

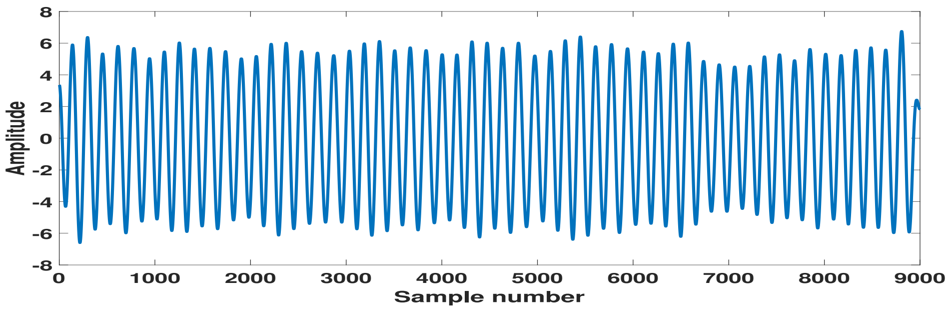

(b)

Figure 3.9: Second epoch (a) Sub-band1 (b) Sub-band2.

Step 5: RR and HR extraction by using FBSE

For first epoch, RR and HR are 18.7506 breaths/min and 114.75 beats/min, respectively.

For second epoch, RR and HR are 16.7508 breaths/min and 112.752 beats/min, respectively.

3.6 Summary

In this work, we have used capnobase and MIMIC databases which are available online and we have proposed FBSE-EWT based approach for the extraction of HR and RR from PPG signals. In, the proposed method FBSE has been used in place of FFT because of higher resolution. After that, scale-space technique has been used for boundary detection of frequency spectrum. Then, EWT based filter bank has been used for sub-bands extraction. In the proposed method, Gaussian filter is used to reduce noise from frequency spectrum. In the proposed method, box-Whisker's plot, Bland-Altman's plot has been used to discuss the results. The proposed method has provided good performance in terms of RMSE and Pearson's correlation as compared to EEMD-PCA, EMD-PCA, and other methods.

Chapter 4

Results and Discussion

In this chapter, we have discussed results of proposed method. Box Whisker's plot, Pearson's plot, Bland-Altman plot, and RMSEs have been discussed using figures and tables. We have shown box Whisker's plot, Pearson's plot, and Bland-Altman plot for both databases. Using RMSEs, results have been compared with existing techniques. We have shown box-whisker plot of HR and RR rate extracted from the reference signal and PPG signal in Figs. 4.1 - 4.4 for MIMIC and capnobase databases, where HR(R) and HR(D), RR(R), RR(D) represent reference HR and PPG calculated HR, reference RR, PPG calculated RR, respectively. We have shown median value for MIMIC and capnobase databases for RR and HR in Table 4.1 for box plots.

Table 4.1: Median, 1st quartile and 3rd quartile value for reference and PPG calculated RR and HR for MIMIC and capnobase databases

Database	RR-Median(1st quartile, 3rd quartile)	HR-Median(1st quartile, 3rd quartile)
$\text{MIMIC}_{\text{Ref}}$	16.89(14.92,18.90)	88.845(108.845,61.9093)
$\text{MIMIC}_{\text{Derived}}$	16.79(14.72,18.90)	88.8902(108.8156,63.2801)
$\text{Capnobase}_{\text{Ref}}$	11.75(9.75,18.75)	101.748(129.765,76.75)
$\text{Capnobase}_{\text{Derived}}$	11.75(10.10,18.75)	101.76(129.765,77.25)

Figs. 4.5 - 4.8 have shown the Pearson scatter plots and Bland-Altman plots. The obtained values of PCC for RR estimation are 0.99 and 0.99 for MIMIC and capnobase databases, respectively. We have achieved Pearson correlation nearly 1 for both datasets so accuracy is good for both datasets. For HR estimation, PCC are 0.86 and 0.88 for MIMIC and capnobase databases, respectively. We have shown Pearson

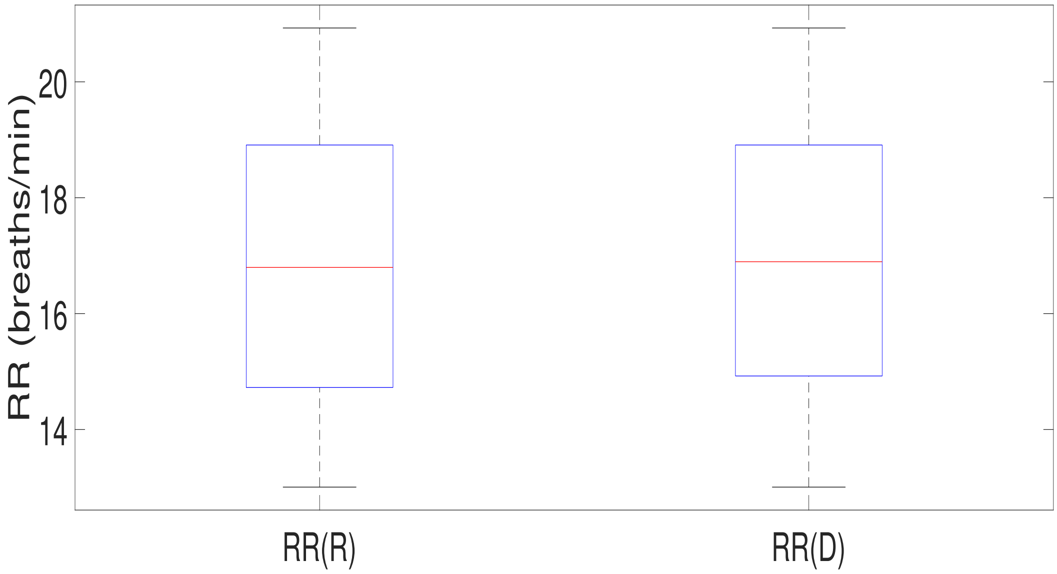

Figure 4.1: Box-Whiskers plot of reference and FBSE-EWT based PPG derived RR for MIMIC dataset.

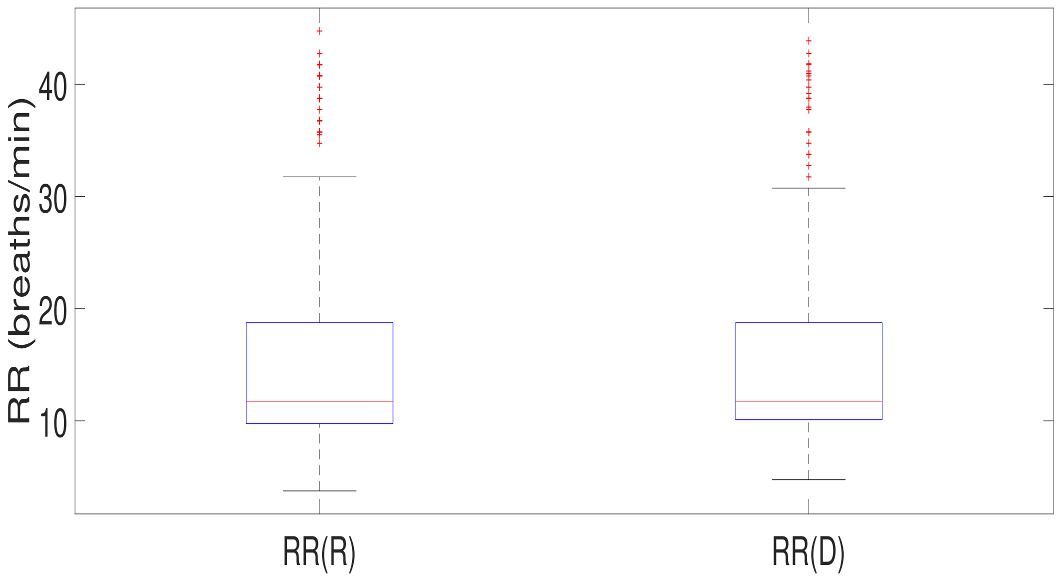

Figure 4.2: Box-Whiskers plot of reference and FBSE-EWT based PPG derived RR for capnobase dataset.

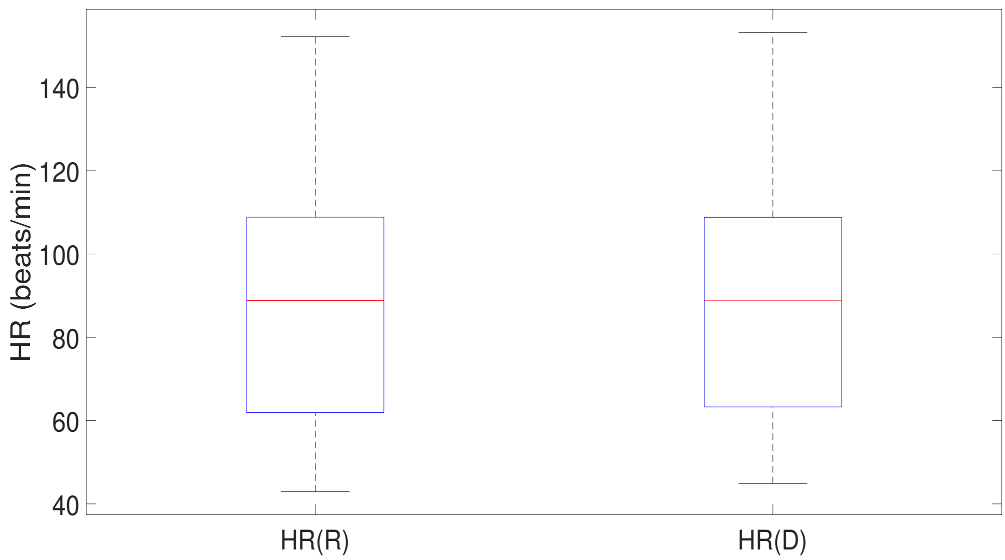

Figure 4.3: Box-Whiskers plot of reference and FBSE-EWT based PPG derived HR for MIMIC dataset.

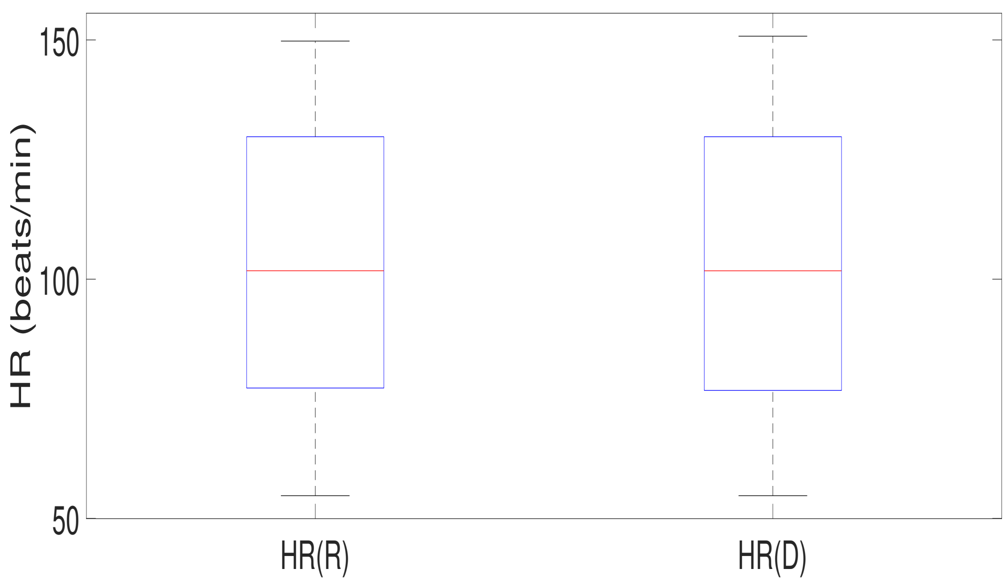

Figure 4.4: Box-Whiskers plot of reference and FBSE-EWT based PPG derived HR for capnobase dataset.

correlation in Table 4.2. In Figs. 4.5 and 4.6, these plots show RR bias of -0.03 and 0.02 along with limits of agreement of -0.56 to 0.49 and -1.7 to 1.7 for MIMIC and capnobase databases, respectively. In Figs. 4.7 and 4.8, these plots show HR bias of 0.88 and 0.02 along with limits of agreement of -4.4 to 6.2 and -2.2 to 2.3 for MIMIC and capnobase databases, respectively.

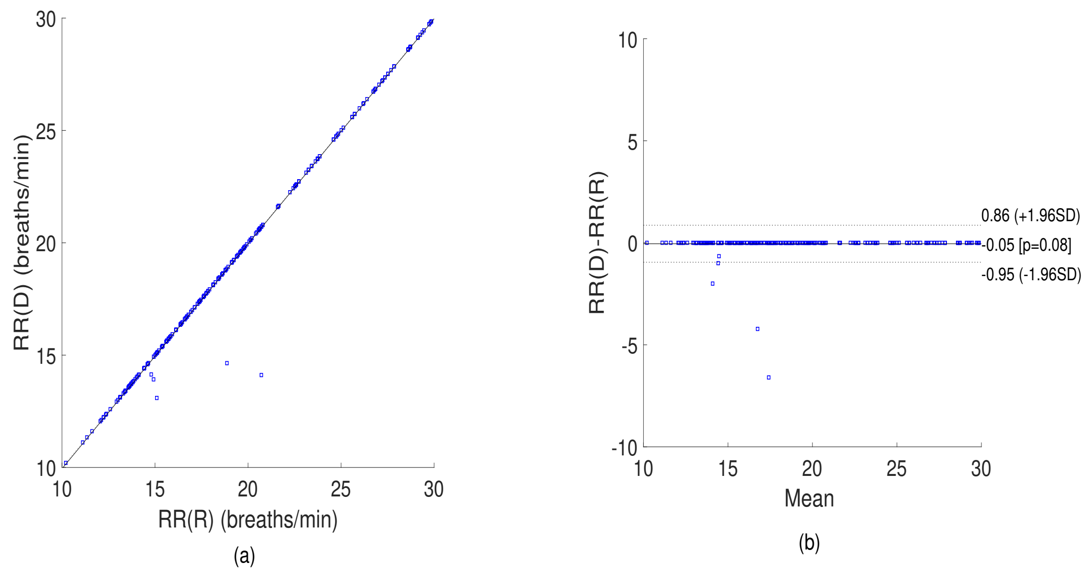

Figure 4.5: Pearson scatter plot and Bland-Altman plot for comparison of derived RR to the reference RR for MIMIC dataset.

Table 4.2: RMS error as median, PCC of PPG derived RR and HR with reference RR and HR for MIMIC and capnobase datasets

Dataset	RMS Error	PCC
MIMIC_{RR}	0.48549	0.99
$\text{Capnobase}_{\text{RR}}$	0.92545	0.99
MIMIC_{HR}	2.39632	0.86
$\text{Capnobase}_{\text{HR}}$	1.444	0.88

In previous work [85], first authors decomposed signal and extracted IMFs. After that, they have applied PCA on IMFs. In our proposed method, we have extracted

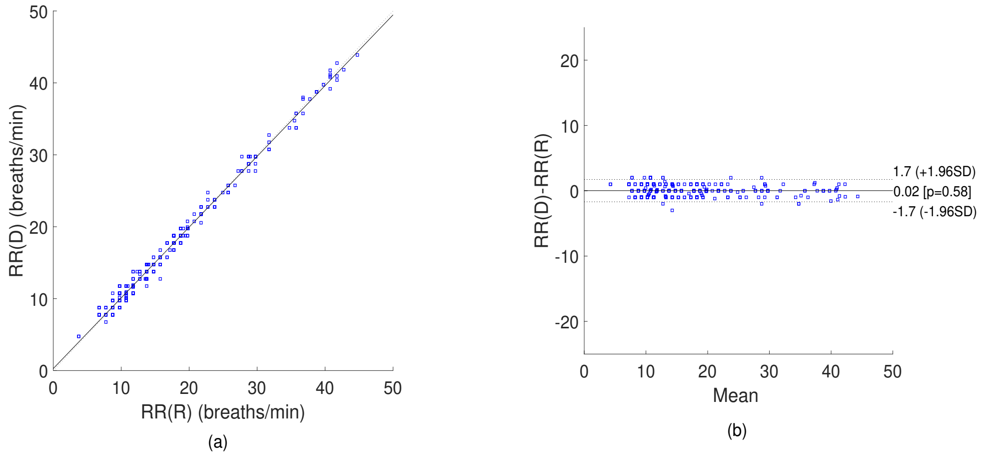

Figure 4.6: Pearson scatter plot and Bland-Altman plot for comparison of derived RR to the reference RR for capnobase dataset.

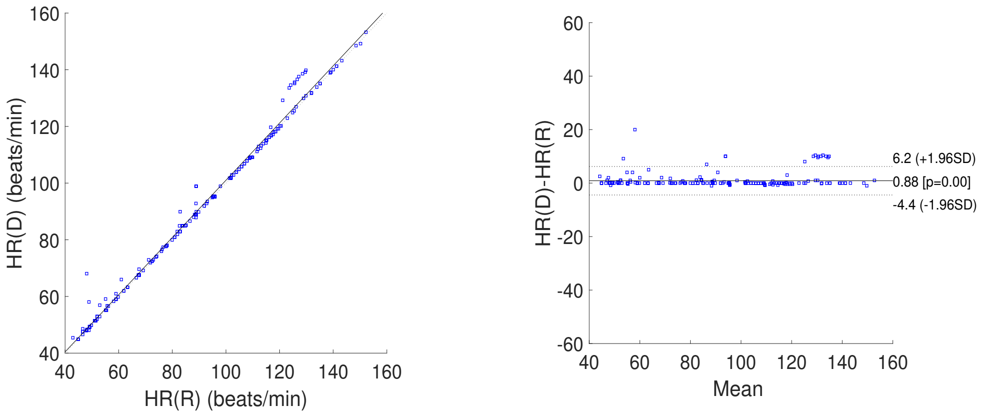

Figure 4.7: Pearson scatter plot and Bland-Altman plot for comparison of derived HR to the reference HR for MIMIC dataset.

sub-bands after application of FBSE-EWT method and we found that only first sub-band and second sub-band are in the range of respiration frequency (0.05-0.75 Hz) and cardiac frequency (0.75-2.5Hz) for each epoch, respectively. After that, we have applied FBSE on that first and second sub-band in order to obtain RR and HR. We have compared our obtained results with existing methods in Table 4.3. In Table 4.3,

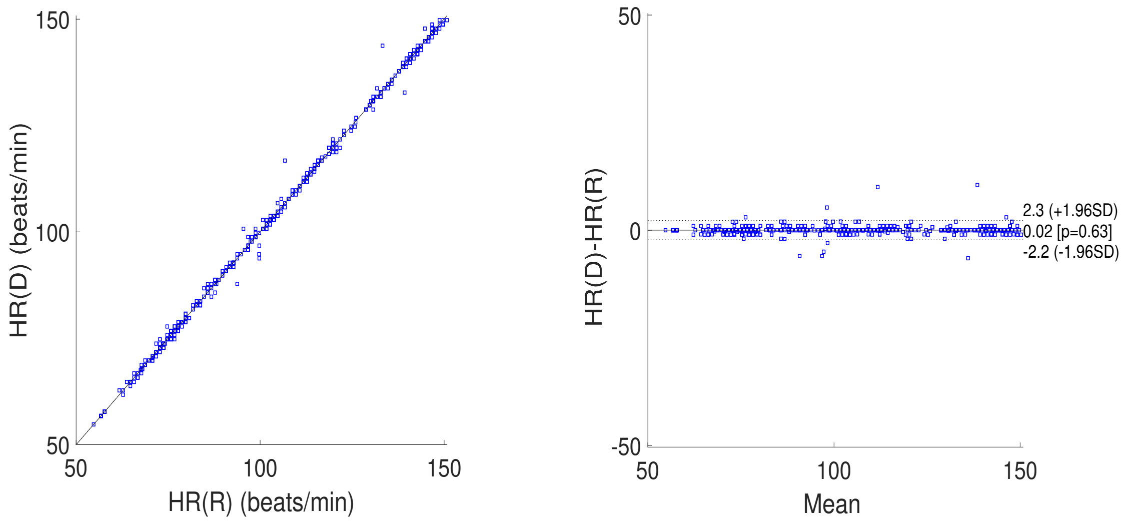

Figure 4.8: Pearson scatter plot and Bland-Altman plot for comparison of derived HR to the reference HR for capnobase dataset.

we have shown our results for both databases, while most of the other techniques have used the single database for validating their algorithms. It should be noted that the data length used in other existing methods is not same for the validation purpose. Hence, we have compared the results of RMSE with data length for each method in Table 4.3. The obtained RMSEs of RR for FBSE-EWT based method are 0.48549 and 0.92545 for MIMIC and capnobase databases, respectively, which are the lowest among the other existing methods. The obtained RMSEs of HR for FBSE-EWT based method are 2.39632 and 1.444 for MIMIC and capnobase databases, respectively. In our proposed work, the first sub-band and second sub-band fall in the range of 0.05-0.75 Hz and 0.75-2.5Hz for both databases, respectively. Hence, we have used first sub-band and second sub-band for the extraction of RR and HR in our proposed method. It should be noted that if more than one sub-band fall in the range of 0.05-0.75 Hz and 0.75-2.5 Hz for the extraction of RR and HR from other databases. Then, our proposed method will require merging of these sub-bands which fall in the frequency range 0.05-0.75 Hz or 0.75-2.5 Hz and mean-frequency parameter [154] can be used

Table 4.3: Comparison of RMSE for PPG derived RR and HR with other existing methods. RMSE represented as median (1st quartile, 3rd quartile)

Methods and databases	RR-RMSE (breaths/min)	HR-RMSE (beats/min)	Data length (sec)
FBSE-EWT (proposed), MIMIC database	0.48549(0.21556,1.3409)	2.39632(1.25,3.4576)	30
FBSE-EWT (proposed), capnobase database	0.92545(0.22349,2.2735)	1.444(0.5,1.542)	30
EEMD-PCA [85], MIMIC database	0.89(0,1.78)	0.57(0.30,0.71)	30
EEMD-PCA [85], capnobase database	2.77(0.50,5.9)	0.69(0.54,1.10)	30
Correntropy spectral density (CSD) [148], capnobase database	0.95(0.27,6.20)	0.76(0.34,1.45)	120
Power spectral density (PSD) [148], capnobase database	3.18(1.20,11.3)	0.58(0.21,1.17)	120
Smart fusion [88], capnobase database	1.56(0.60,3.15)	n/a	32
EMD [83], capnobase database	3.5(1.1,11)	0.35(0.2,0.59)	60

due to narrow band nature of these sub-bands in order to determine the sub-bands corresponding to this range.

Chapter 5

Conclusions and Future work

5.1 Conclusions

We have presented a new FBSE-EWT method for extraction of HR and RR from PPG signals. FBSE spectrum is used for optimum border frequency estimation. Afterwards, the scale-spaced technique for detecting the spectrum limits has been employed. After that, EWT based filter bank has been applied for the extraction of sub-bands. In previous techniques, most of the authors have used single database to validate their technique. In proposed technique, both databases have been used to validate proposed algorithm. Most of the authors have used long duration dataset but we have used short data length which is equal to 30 seconds.

5.2 Future work

In this thesis, we have proposed a method to estimate RR and HR from PPG signals. Most of the methods have been used long data length greater than 30 seconds for the estimation of RR from PPG signals. However, our proposed method has applied on both databases for short data length which is equal to 30 seconds. In the proposed method there is no need for filtering of IMFs and no need of grouping of IMFs. Hence, the proposed method requires less computational complexity. Furthermore, the proposed method requires testing on large number of PPG signal databases before it to be used in healthcare. In future, we can apply this method on very short data length less than 30 seconds for the estimation of RR and HR which further reduces the computational complexity of the proposed method. The proposed method can be modified for other biomedical signals analysis and classification.

REFERENCES

[1] Y. Mendelson, "Pulse oximetry: theory and applications for noninvasive monitoring." *Clinical Chemistry*, vol. 38, no. 9, pp. 1601–1607, 1992.

[2] Z. Taha, L. Shirley, and M. A. M. Razman, "A review on non-invasive hypertension monitoring system by using photoplethysmography method," *Malaysian Journal of Movement, Health & Exercise*, vol. 6, no. 1, 2017.

[3] J. Moraes, M. Rocha, G. Vasconcelos, J. Vasconcelos Filho, V. de Albuquerque, and A. Alexandria, "Advances in photopletysmography signal analysis for biomedical applications," *Sensors*, vol. 18, no. 6, p. 1894, 2018.

[4] Z. Zhao, L. Yang, D. Chen, and Y. Luo, "A human ECG identification system based on ensemble empirical mode decomposition," *Sensors*, vol. 13, no. 5, pp. 6832–6864, 2013.

[5] A. A. Alian and K. H. Shelley, "Photoplethysmography," *Best Practice & Research Clinical Anaesthesiology*, vol. 28, no. 4, pp. 395–406, 2014.

[6] E. B. Blackford, A. M. Piasecki, and J. R. Estepp, "Measuring pulse rate variability using long-range, non-contact imaging photoplethysmography," in *2016 38th Annual International Conference of the IEEE Engineering in Medicine and Biology Society (EMBC).* IEEE, 2016, pp. 3930–3936.

[7] K. Suwa, "Pulse oximetry , 2nd ed., by jtb moyle (bmj, london, uk, 2002. 174 pp. £19.95. isbn 0-7279-1740-4)," *Journal of Anesthesia - J ANESTH*, vol. 17, pp. 74–74, 02 2003.

[8] E. Gil, M. Orini, R. Bailón, J. M. Vergara, L. Mainardi, and P. Laguna, "Photoplethysmography pulse rate variability as a surrogate measurement of heart rate variability during non-stationary conditions," *Physiological Measurement*, vol. 31, no. 9, p. 1271, 2010.

[9] J. Allen and A. Murray, "Modelling the relationship between peripheral blood pressure and blood volume pulses using linear and neural network system identification techniques," *Physiological Measurement*, vol. 20, no. 3, p. 287, 1999.

[10] S. C. Millasseau, F. G. Guigui, R. P. Kelly, K. Prasad, J. R. Cockcroft, J. M. Ritter, and P. J. Chowienczyk, "Noninvasive assessment of the digital volume pulse: comparison with the peripheral pressure pulse," *Hypertension*, vol. 36, no. 6, pp. 952–956, 2000.

[11] J. Penaz, "Photoelectric measurement of blood pressure, volume and flow in the finger'in: Digest of the 10th international conference on medical and biological engineering," *Dresden*, vol. 104, 1973.

[12] G. Madhavan, "Plethysmography," *Biomedical Instrumentation & Technology*, vol. 39, no. 5, pp. 367–371, 2005.

[13] J. Allen, "Photoplethysmography and its application in clinical physiological measurement," *Physiological Measurement*, vol. 28, no. 3, p. R1, 2007.

[14] J. Bhattacharya, P. P. Kanjilal, and V. Muralidhar, "Analysis and characterization of photo-plethysmographic signal," *IEEE Transactions on Biomedical Engineering*, vol. 48, no. 1, pp. 5–11, 2001.

[15] N. Westerhof, N. Stergiopulos, and M. I. Noble, "Transfer of pressure," in *Snapshots of Hemodynamics*. Springer, 2010, pp. 189–195.

[16] W. Welkowitz, "Engineering hemodynamics: Application to cardiac assist devices," *Journal of Clinical Engineering*, vol. 13, no. 2, p. 79, 1988.

[17] L. Cotton, C. Roberts, and F. Cave, "Value of the electromagnetic flowmeter in arterial reconstruction," *Blood Flow Measurement. London, Sector Publishing Ltd*, pp. 107–110, 1972.

[18] L. Hejjel and I. Gal, "Heart rate variability analysis," *Acta Physiologica Hungarica*, vol. 88, no. 3-4, pp. 219–230, 2001.

[19] L. Ø. Høiseth, I. E. Hoff, O. A. Hagen, K. A. Kirkebøen, and S. A. Landsverk, "Respiratory variations in the photoplethysmographic waveform amplitude depend on type of pulse oximetry device," *Journal of Clinical Monitoring and Computing*, vol. 30, no. 3, pp. 317–325, 2016.

[20] M. C. Hemon and J. P. Phillips, "Comparison of foot finding methods for deriving instantaneous pulse rates from photoplethysmographic signals," *Journal of Clinical Monitoring and Computing*, vol. 30, no. 2, pp. 157–168, 2016.

[21] D. B. McCombie, A. T. Reisner, and H. H. Asada, "Adaptive blood pressure estimation from wearable PPG sensors using peripheral artery pulse wave velocity measurements and multi-channel blind identification of local arterial dynamics," in *2006 International Conference of the IEEE Engineering in Medicine and Biology Society*. IEEE, 2006, pp. 3521–3524.

[22] D. Zhao, Y. Sun, S. Wan, and F. Wang, "Sfst: A robust framework for heart rate monitoring from photoplethysmography signals during physical activities," *Biomedical Signal Processing and Control*, vol. 33, pp. 316–324, 2017.

[23] V. H. C. de Albuquerque, T. M. Nunes, D. R. Pereira, E. J. d. S. Luz, D. Menotti, J. P. Papa, and J. M. R. Tavares, "Robust automated cardiac arrhythmia detection in ECG beat signals," *Neural Computing and Applications*, vol. 29, no. 3, pp. 679–693, 2018.

[24] J. Allen and A. Murray, "Similarity in bilateral photoplethysmographic peripheral pulse wave characteristics at the ears, thumbs and toes," *Physiological Measurement*, vol. 21, no. 3, p. 369, 2000.

[25] Y. Mendelson, R. Duckworth, and G. Comtois, "A wearable reflectance pulse oximeter for remote physiological monitoring," in *2006 International Conference of the IEEE Engineering in Medicine and Biology Society.* IEEE, 2006, pp. 912–915.

[26] D. Meredith, D. Clifton, P. Charlton, J. Brooks, C. Pugh, and L. Tarassenko, "Photoplethysmographic derivation of respiratory rate: a review of relevant physiology," *Journal of Medical Engineering & Technology*, vol. 36, no. 1, pp. 1–7, 2012.

[27] A. Relente and L. Sison, "Characterization and adaptive filtering of motion artifacts in pulse oximetry using accelerometers," in *Proceedings of the Second Joint 24th Annual Conference and the Annual Fall Meeting of the Biomedical Engineering Society][Engineering in Medicine and Biology*, vol. 2. IEEE, 2002, pp. 1769–1770.

[28] W. Karlen, S. Raman, J. M. Ansermino, and G. A. Dumont, "Multiparameter respiratory rate estimation from the photoplethysmogram," *IEEE Transactions on Biomedical Engineering*, vol. 60, no. 7, pp. 1946–1953, 2013.

[29] J. G. Webster, *Design of pulse oximeters.* CRC Press, 1997.

[30] T. D. Pham and M. Oyama-Higa, "Photoplethysmography technology and its feature visualization for cognitive stimulation assessment," in *2015 IEEE International Conference on Industrial Technology (ICIT).* IEEE, 2015, pp. 1735–1740.

[31] H. Lee, H. Chung, H. Ko, and J. Lee, "Wearable multichannel photoplethysmography framework for heart rate monitoring during intensive exercise," *IEEE Sensors Journal*, vol. 18, no. 7, pp. 2983–2993, 2018.

[32] G. S. Ling, K. Day, P. Rhee, and J. M. Ecklund, "In search of technological solutions to battlefield management of combat casualties," in *Battlefield Biomedical Technologies*, vol. 3712. International Society for Optics and Photonics, 1999, pp. 1–9.

[33] J. Obusek, "Warfighter physiological status monitoring," *The Warrior*, pp. 6–8, 2001.

[34] S. Patidar and R. B. Pachori, "Classification of cardiac sound signals using constrained tunable-Q wavelet transform," *Expert Systems with Applications*, vol. 41, no. 16, pp. 7161 – 7170, 2014.

[35] H. Husum, M. Gilbert, T. Wisborg, Y. Van Heng, and M. Murad, "Respiratory rate as a prehospital triage tool in rural trauma," *Journal of Trauma and Acute Care Surgery*, vol. 55, no. 3, pp. 466–470, 2003.

[36] S. C. Tarrant, R. E. Ellis, F. C. Flack, and W. G. Selley, "Comparative review of techniques for recording respiratory events at rest and during deglutition," *Dysphagia*, vol. 12, no. 1, pp. 24–38, 1997.

[37] K. P. Cohen, D. Panescu, J. H. Booske, J. G. Webster, and W. J. Tompkins, "Design of an inductive plethysmograph for ventilation measurement," *Physiological Measurement*, vol. 15, no. 2, p. 217, 1994.

[38] W. Johnston and Y. Mendelson, "Extracting breathing rate information from a wearable reflectance pulse oximeter sensor," in *The 26th Annual International Conference of the IEEE Engineering in Medicine and Biology Society*, vol. 2. IEEE, 2004, pp. 5388–5391.

[39] J. Lee, W. Jung, I. Kang, Y. Kim, and G. Lee, "Design of filter to reject motion artifact of pulse oximetry," *Computer Standards & Interfaces*, vol. 26, no. 3, pp. 241–249, 2004.

[40] H.-W. Lee, J.-W. Lee, W.-G. Jung, and G.-K. Lee, "The periodic moving average filter for removing motion artifacts from PPG signals," *International Journal of Control, Automation, and Systems*, vol. 5, no. 6, pp. 701–706, 2007.

[41] L. M. Ruiz, A. Manzo, E. Casimiro, E. Cárdenas, and R. González, "Heart rate variability using photoplethysmography with green wavelength," in *2014 IEEE International Autumn Meeting on Power, Electronics and Computing (ROPEC)*. IEEE, 2014, pp. 1–5.

[42] L. Manonelles Rincón, "Development of an acquisition circuit of multiple biological signals for integration into a wearable bracelet," B.S. thesis, Universitat Politècnica de Catalunya, 2017.

[43] R. Kukkapalli, *Non-invasive wearable sensors for respiration monitoring.* University of Maryland, Baltimore County, 2016.

[44] H. Asada, A. Reisner, P. Shaltis, and D. McCombie, "Towards the development of wearable blood pressure sensors: a photo-plethysmograph approach using conducting polymer actuators," in *2005 IEEE Engineering in Medicine and Biology 27th Annual Conference.* IEEE, 2005, pp. 4156–4159.

[45] P. K. Baheti and H. Garudadri, "An ultra low power pulse oximeter sensor based on compressed sensing," in *2009 Sixth International Workshop on Wearable and Implantable Body Sensor Networks.* IEEE, 2009, pp. 144–148.

[46] L. Wang, B. P. Lo, and G.-Z. Yang, "Multichannel reflective PPG earpiece sensor with passive motion cancellation," *IEEE Transactions on Biomedical Circuits and Systems*, vol. 1, no. 4, pp. 235–241, 2007.

[47] S. Rhee and S. Liu, "An ultra-low power, self-organizing wireless network and non-invasive biomedical instrumentation," in *Proceedings of the Second Joint 24th Annual Conference and the Annual Fall Meeting of the Biomedical Engineering Society][Engineering in Medicine and Biology*, vol. 3. IEEE, 2002, pp. 1803–1804.

[48] K. Nakajima, T. Tamura, T. Ohta, H. Miike, and P. Oberg, "Photoplethysmographic measurement of heart and respiratory rates using digital filters," in *Proceedings of the 15th Annual International Conference of the IEEE Engineering in Medicine and Biology Societ.* IEEE, 1993, pp. 1006–1007.

[49] K. Nakajima, T. Tamura, and H. Miike, "Monitoring of heart and respiratory rates by photoplethysmography using a digital filtering technique," *Medical Engineering & Physics*, vol. 18, no. 5, pp. 365–372, 1996.

[50] T. Oberlin, S. Meignen, and V. Perrier, "The Fourier-based synchrosqueezing transform," in *2014 IEEE International Conference on Acoustics, Speech and Signal Processing (ICASSP)*. IEEE, 2014, pp. 315–319.

[51] O. Poisson, P. Rioual, and M. Meunier, "New signal processing tools applied to power quality analysis," *IEEE Transactions on Power Delivery*, vol. 14, no. 2, pp. 561–566, 1999.

[52] J. F. Thayer, J. J. Sollers, E. Ruiz-Padial, and J. Vila, "Estimating respiratory frequency from autoregressive spectral analysis of heart period," *IEEE Engineering in Medicine and Biology Magazine*, vol. 21, no. 4, pp. 41–45, 2002.

[53] M. S. Arulampalam, S. Maskell, N. Gordon, and T. Clapp, "A tutorial on particle filters for online nonlinear/non-Gaussian Bayesian tracking," *IEEE Transactions on Signal Processing*, vol. 50, no. 2, pp. 174–188, 2002.

[54] J. Lázaro Plaza, "Non-invasive techniques for respiratory information extraction based on pulse photoplethysmogram and electrocardiogram," Tech. Rep., 2015.

[55] A. Doucet and A. M. Johansen, "A tutorial on particle filtering and smoothing: Fifteen years later," *Handbook of Nonlinear Filtering*, vol. 12, no. 656-704, p. 3, 2009.

[56] K. H. Shelley, A. A. Awad, R. G. Stout, and D. G. Silverman, "The use of joint time frequency analysis to quantify the effect of ventilation on the pulse oximeter waveform," *Journal of Clinical Monitoring and Computing*, vol. 20, no. 2, pp. 81–87, 2006.

[57] T. Li, M. Bolic, and P. M. Djuric, "Resampling methods for particle filtering: classification, implementation, and strategies," *IEEE Signal Processing Magazine*, vol. 32, no. 3, pp. 70–86, 2015.

[58] R. Bailón, D. Habas, L. Sornmo, and P. Laguna, "Robust estimation of respiratory frequency from exercise ECGs," in *Computers in Cardiology, 2003*. IEEE, 2003, pp. 299–302.

[59] V. Jeyhani, T. Vuorinen, M. Mäntysalo, and A. Vehkaoja, “Comparison of simple algorithms for estimating respiration rate from electrical impedance pneumography signals in wearable devices,” *Health and Technology*, vol. 7, no. 1, pp. 21–31, 2017.

[60] X. Zhang and Q. Ding, “Respiratory rate estimation from the photoplethysmogram via joint sparse signal reconstruction and spectra fusion,” *Biomedical Signal Processing and Control*, vol. 35, pp. 1–7, 2017.

[61] Zhang, Xiaorong and Ding, Quan, “Respiratory rate monitoring from the photoplethysmogram via sparse signal reconstruction,” *Physiological Measurement*, vol. 37, no. 7, p. 1105, 2016.

[62] P. S. Addison and J. N. Watson, “Secondary transform decoupling of shifted nonstationary signal modulation components: Application to photoplethysmography,” *International Journal of Wavelets, Multiresolution and Information Processing*, vol. 02, no. 01, pp. 43–57, 2004.

[63] H. Yang, “Synchrosqueezed wave packet transforms and diffeomorphism based spectral analysis for 1d general mode decompositions,” *Applied and Computational Harmonic Analysis*, vol. 39, no. 1, pp. 33–66, 2015.

[64] S. Gupta and J. B. Sharma, “Estimation of respiratory rate from the ECG using instantaneous frequency tracking lms algorithm,” in *2016 2nd International Conference on Advances in Computing, Communication, Automation (ICACCA) (Fall)*, 2016, pp. 1–5.

[65] J. Lee and K. H. Chon, “An autoregressive model-based particle filtering algorithms for extraction of respiratory rates as high as 90 breaths per minute from pulse oximeter,” *IEEE Transactions on Biomedical Engineering*, vol. 57, no. 9, pp. 2158–2167, 2010.

[66] A. Cicone and H.-T. Wu, “How nonlinear-type time-frequency analysis can help in sensing instantaneous heart rate and instantaneous respiratory rate from pho-

toplethysmography in a reliable way," *Frontiers in Physiology*, vol. 8, p. 701, 2017.

[67] H. Kim, J.-Y. Kim, and C.-H. Im, "Fast and robust real-time estimation of respiratory rate from photoplethysmography," *Sensors*, vol. 16, no. 9, 2016.

[68] C. Park and B. Lee, "Real-time estimation of respiratory rate from a photoplethysmogram using an adaptive lattice notch filter," *BioMedical Engineering OnLine*, vol. 13, no. 1, p. 170, Dec 2014.

[69] L. Mirmohamadsadeghi and J.-M. Vesin, "Respiratory rate estimation from the ECG using an instantaneous frequency tracking algorithm," *Biomedical Signal Processing and Control*, vol. 14, pp. 66 – 72, 2014.

[70] K. V. Madhav, M. Raghuram, E. H. Krishna, N. R. Komalla, and K. A. Reddy, "Extraction of respiratory activity from ECG and PPG signals using vector autoregressive model," in *2012 IEEE International Symposium on Medical Measurements and Applications Proceedings.* IEEE, 2012, pp. 1–4.

[71] L. Mirmohamadsadeghi and J.-M. Vesin, "Real-time multi-signal frequency tracking with a bank of notch filters to estimate the respiratory rate from the ECG," *Physiological Measurement*, vol. 37, no. 9, pp. 1573–1587, aug 2016.

[72] L. Mirmohamadsadeghi and J. Vesin, "Estimating the real-time respiratory rate from the ecg with a bank of notch filters," in *2015 Computing in Cardiology Conference (CinC)*, Sep. 2015, pp. 581–584.

[73] D. Cvetkovic, E. D. Übeyli, and I. Cosic, "Wavelet transform feature extraction from human PPG, ECG, and EEG signal responses to elf pemf exposures: A pilot study," *Digital Signal Processing*, vol. 18, no. 5, pp. 861–874, 2008.

[74] S. Fleming, L. Tarassenko, M. Thompson, and D. Mant, "Non-invasive measurement of respiratory rate in children using the photoplethysmogram," in *2008 30th Annual International Conference of the IEEE Engineering in Medicine and Biology Society*, Aug 2008, pp. 1886–1889.

[75] S. Moreno, A. Quintero-Parra, C. Ochoa-Pertuz, R. Villarreal, and I. Kuzmar, "A signal processing method for respiratory rate estimation through photoplethysmography," *International Journal of Signal Processing, Image Processing and Pattern Recognition*, vol. 11, no. 2, pp. 1–10, 2018.

[76] K. V. Madhav, M. Raghuram, E. H. Krishna, N. R. Komalla, and K. A. Reddy, "Use of multi scale pca for extraction of respiratory activity from photoplethysmographic signals," in *2012 IEEE International Instrumentation and Measurement Technology Conference Proceedings*. IEEE, 2012, pp. 1784–1787.

[77] S. Dash, K. H. Shelley, D. G. Silverman, and K. H. Chon, "Estimation of respiratory rate from ECG, photoplethysmogram, and piezoelectric pulse transducer signals: a comparative study of time–frequency methods," *IEEE Transactions on Biomedical Engineering*, vol. 57, no. 5, pp. 1099–1107, 2010.

[78] P. A. Leonard, J. G. Douglas, N. R. Grubb, D. Clifton, P. S. Addison, and J. N. Watson, "A fully automated algorithm for the determination of respiratory rate from the photoplethysmogram," *Journal of Clinical Monitoring and Computing*, vol. 20, no. 1, pp. 33–36, 2006.

[79] H.-T. Wu, Y.-H. Chan, Y.-T. Lin, and Y.-H. Yeh, "Using synchrosqueezing transform to discover breathing dynamics from ECG signals," *Applied and Computational Harmonic Analysis*, vol. 36, no. 2, pp. 354–359, 2014.

[80] M. Pirhonen, O. Suominen, and A. Vehkaoja, "Auto-regression-driven, reallocative particle filtering approaches in PPG-based respiration rate estimation," in *EMBEC & NBC 2017*. Springer, 2017, pp. 1020–1024.

[81] K. H. Chon, S. Dash, and K. Ju, "Estimation of respiratory rate from photoplethysmogram data using time–frequency spectral estimation," *IEEE Transactions on Biomedical Engineering*, vol. 56, no. 8, pp. 2054–2063, 2009.

[82] D. Labate, F. La Foresta, G. Occhiuto, F. C. Morabito, A. Lay-Ekuakille, and P. Vergallo, "Empirical mode decomposition vs. wavelet decomposition for the

extraction of respiratory signal from single-channel ECG: A comparison," *IEEE Sensors Journal*, vol. 13, no. 7, pp. 2666–2674, 2013.

[83] A. Garde, W. Karlen, P. Dehkordi, J. Ansermino, and G. Dumont, "Empirical mode decomposition for respiratory and heart rate estimation from the photoplethysmogram," in *Computing in Cardiology 2013*, Sep. 2013, pp. 799–802.

[84] D. Li, H. Zhao, and S. Dou, "A new signal decomposition to estimate breathing rate and heart rate from photoplethysmography signal," *Biomedical Signal Processing and Control*, vol. 19, pp. 89–95, 2015.

[85] M. A. Motin, C. K. Karmakar, and M. Palaniswami, "Ensemble empirical mode decomposition with principal component analysis: A novel approach for extracting respiratory rate and heart rate from photoplethysmographic signal," *IEEE Journal of Biomedical and Health Informatics*, vol. 22, no. 3, pp. 766–774, May 2018.

[86] K. V. Madhav, M. R. Ram, E. H. Krishna, N. R. Komalla, and K. A. Reddy, "Robust extraction of respiratory activity from PPG signals using modified MSPCA," *IEEE Transactions on Instrumentation and Measurement*, vol. 62, no. 5, pp. 1094–1106, 2013.

[87] L. Nilsson, A. Johansson, and S. Kalman, "Monitoring of respiratory rate in postoperative care using a new photoplethysmographic technique," *Journal of Clinical Monitoring and Computing*, vol. 16, no. 4, pp. 309–315, 2000.

[88] W. Karlen, S. Raman, J. M. Ansermino, and G. A. Dumont, "Multiparameter respiratory rate estimation from the photoplethysmogram," *IEEE Transactions on Biomedical Engineering*, vol. 60, no. 7, pp. 1946–1953, July 2013.

[89] M. A. Motin, C. K. Karmakar, and M. Palaniswami, "An EEMD-PCA approach to extract heart rate, respiratory rate and respiratory activity from ppg signal," in *2016 38th Annual International Conference of the IEEE Engineering in Medicine and Biology Society (EMBC)*. IEEE, 2016, pp. 3817–3820.

[90] M. Ragab, O. A. Omer, and M. Abdel-Nasser, "Compressive sensing MRI reconstruction using empirical wavelet transform and grey wolf optimizer," *Neural Computing and Applications*, Oct 2018.

[91] E. Cavanagh and B. Cook, "Numerical evaluation of Hankel transforms via Gaussian-Laguerre polynomial expansions," *IEEE Transactions on Acoustics, Speech, and Signal Processing*, vol. 27, no. 4, pp. 361–366, 1979.

[92] J. Schroeder, "Signal processing via Fourier-Bessel series expansion," *Digital Signal Processing*, vol. 3, no. 2, pp. 112 – 124, 1993.

[93] R. B. Pachori and P. Sircar, "EEG signal analysis using FB expansion and second-order linear TVAR process," *Signal Processing*, vol. 88, no. 2, pp. 415–420, 2008.

[94] R. B. Pachori and P. Sircar, "Analysis of multicomponent AM-FM signals using FB-DESA method," *Digital Signal Processing*, vol. 20, no. 1, pp. 42 – 62, 2010.

[95] R. B. Pachori and P. Sircar, "A new technique to reduce cross terms in the Wigner distribution," *Digital Signal Processing*, vol. 17, no. 2, pp. 466–474, 2007.

[96] A. Bhattacharyya, L. Singh, and R. B. Pachori, "Fourier–Bessel series expansion based empirical wavelet transform for analysis of non-stationary signals," *Digital Signal Processing*, vol. 78, pp. 185 – 196, 2018.

[97] A. Bhattacharyya, M. Sharma, R. B. Pachori, P. Sircar, and U. R. Acharya, "A novel approach for automated detection of focal EEG signals using empirical wavelet transform," *Neural Computing and Applications*, vol. 29, no. 8, pp. 47–57, Apr 2018.

[98] R. R. Sharma, P. Chandra, and R. B. Pachori, "Electromyogram signal analysis using eigenvalue decomposition of the Hankel matrix," in *Machine Intelligence and Signal Analysis*, M. Tanveer and R. B. Pachori, Eds. Singapore: Springer Singapore, 2019, pp. 671–682.

[99] A. Nishad, A. Upadhyay, R. B. Pachori, and U. R. Acharya, "Automated classification of hand movements using tunable-Q wavelet transform based filter-bank with surface electromyogram signals," *Future Generation Computer Systems*, vol. 93, pp. 96–110, 2019.

[100] R. B. Pachori and P. Sircar, "EEG signal analysis using FB expansion and second-order linear TVAR process," *Signal Processing*, vol. 88, no. 2, pp. 415 – 420, 2008.

[101] A. Bhattacharyya, R. B. Pachori, and U. R. Acharya, "Tunable-Q wavelet transform based multivariate sub-band fuzzy entropy with application to focal EEG signal analysis," *Entropy*, vol. 19, no. 3, 2017.

[102] V. Gupta, A. Bhattacharyya, and R. B. Pachori, "Automated identification of epileptic seizures from EEG signals using FBSE-EWT method," *Biomedical Signal Processing-Advances in Theory, Algorithms and Applications, Springer*, 2019.

[103] C. Chen, K. Gopalan, and P. Mitra, "Speech signal analysis and synthesis via Fourier-Bessel representation," in *ICASSP'85. IEEE International Conference on Acoustics, Speech, and Signal Processing*, vol. 10. IEEE, 1985, pp. 497–500.

[104] K. Gopalan and C. Chen, "Numerical evaluation of Fourier-Bessel series expansion," in *ICASSP'83. IEEE International Conference on Acoustics, Speech, and Signal Processing*, vol. 8. IEEE, 1983, pp. 151–154.

[105] R. B. Pachori and P. Sircar, "Speech analysis using Fourier-Bessel expansion and discrete energy separation algorithm," in *2006 IEEE 12th Digital Signal Processing Workshop & 4th IEEE Signal Processing Education Workshop.* IEEE, 2006, pp. 423–428.

[106] J. Bird and D. George, "The use of the Fourier-Bessel series in calculating error probabilities for digital communication systems," *IEEE Transactions on Communications*, vol. 29, no. 9, pp. 1357–1365, 1981.

[107] M. Sharma, P. Achuth, R. B. Pachori, and V. M. Gadre, "A parametrization technique to design joint time–frequency optimized discrete-time biorthogonal wavelet bases," *Signal Processing*, vol. 135, pp. 107 – 120, 2017.

[108] A. Bhattacharyya, R. B. Pachori, A. Upadhyay, and U. R. Acharya, "Tunable-Q wavelet transform based multiscale entropy measure for automated classification of epileptic EEG signals," *Applied Sciences*, vol. 7, no. 4, 2017.

[109] A. Bhattacharyya, L. Singh, and R. B. Pachori, "Identification of epileptic seizures from scalp EEG signals based on TQWT," in *Machine Intelligence and Signal Analysis*, M. Tanveer and R. B. Pachori, Eds. Singapore: Springer Singapore, 2019, pp. 209–221.

[110] A. Nishad, R. B. Pachori, and U. R. Acharya, "Application of TQWT based filter-bank for sleep apnea screening using ECG signals," *Journal of Ambient Intelligence and Humanized Computing*, pp. 1–12, 2018.

[111] J. Gilles, "Empirical wavelet transform," *IEEE Transactions on Signal Processing*, vol. 61, no. 16, pp. 3999–4010, Aug 2013.

[112] J. Gilles, G. Tran, and S. Osher, "2d empirical transforms. wavelets, ridgelets, and curvelets revisited," *SIAM Journal on Imaging Sciences*, vol. 7, no. 1, pp. 157–186, 2014.

[113] A. Witkin, "Scale-space filtering: A new approach to multi-scale description," in *ICASSP'84. IEEE International Conference on Acoustics, Speech, and Signal Processing*, vol. 9. IEEE, 1984, pp. 150–153.

[114] J. J. Koenderink, "The structure of images," *Biological cybernetics*, vol. 50, no. 5, pp. 363–370, 1984.

[115] V. Gupta, T. Priya, A. K. Yadav, R. B. Pachori, and U. R. Acharya, "Automated detection of focal EEG signals using features extracted from flexible analytic wavelet transform," *Pattern Recognition Letters*, vol. 94, pp. 180–188, 2017.

[116] A. Upadhyay and R. B. Pachori, "Instantaneous voiced/non-voiced detection in speech signals based on variational mode decomposition," *Journal of the Franklin Institute*, vol. 352, no. 7, pp. 2679 – 2707, 2015.

[117] P. Maragos, J. F. Kaiser, and T. F. Quatieri, "Energy separation in signal modulations with application to speech analysis," *IEEE Transactions on Signal Processing*, vol. 41, no. 10, pp. 3024–3051, 1993.

[118] J. Weickert, S. Ishikawa, and A. Imiya, "Linear scale-space has first been proposed in japan," *Journal of Mathematical Imaging and Vision*, vol. 10, no. 3, pp. 237–252, May 1999.

[119] A. Nishad and R. B. Pachori, "Instantaneous fundamental frequency estimation of speech signals using tunable-Q wavelet transform," in *2018 International Conference on Signal Processing and Communications (SPCOM)*. IEEE, 2018, pp. 157–161.

[120] V. Gupta, A. Nishad, and R. B. Pachori, "Focal EEG signal detection based on constant-bandwidth TQWT filter-banks," in *2018 IEEE International Conference on Bioinformatics and Biomedicine (BIBM)*. IEEE, 2018, pp. 2597–2604.

[121] N. Otsu, "A threshold selection method from gray-level histograms," *IEEE Transactions on Systems, Man, and Cybernetics*, vol. 9, no. 1, pp. 62–66, Jan 1979.

[122] F. Mokhtarian and M. Bober, *Curvature scale space representation: theory, applications, and MPEG-7 standardization*. Springer Science & Business Media, 2013, vol. 25.

[123] J. Gilles and K. Heal, "A parameterless scale-space approach to find meaningful modes in histograms — application to image and spectrum segmentation," *International Journal of Wavelets, Multiresolution and Information Processing*, vol. 12, no. 06, p. 1450044, 2014.

[124] T. Li and Y. Tang, "Frequency estimation based on modulation FFT and music algorithm," in *2010 First International Conference on Pervasive Computing, Signal Processing and Applications.* IEEE, 2010, pp. 525–528.

[125] A. Bhattacharyya, V. Gupta, and R. B. Pachori, "Automated identification of epileptic seizure EEG signals using empirical wavelet transform based Hilbert marginal spectrum," in *2017 22nd International Conference on Digital Signal Processing (DSP).* IEEE, 2017, pp. 1–5.

[126] S. Candel, "An algorithm for the Fourier-Bessel transform," *Computer physics communications*, vol. 23, no. 4, pp. 343–353, 1981.

[127] Candel, "Dual algorithms for fast calculation of the Fourier-Bessel transform," *IEEE Transactions on Acoustics, Speech, and Signal Processing*, vol. 29, no. 5, pp. 963–972, 1981.

[128] V. Gupta, A. Bhattacharyya, and R. B. Pachori, "Classification of seizure and non-seizure EEG signals based on EMD-TQWT method," in *2017 22nd International Conference on Digital Signal Processing (DSP).* IEEE, 2017, pp. 1–5.

[129] A. S. Hood, R. B. Pachori, V. K. Reddy, and P. Sircar, "Parametric representation of speech employing multi-component AFM signal model," *International Journal of Speech Technology*, vol. 18, no. 3, pp. 287–303, 2015.

[130] V. Gupta, M. D. Chopda, and R. B. Pachori, "Cross-subject emotion recognition using flexible analytic wavelet transform from EEG signals," *IEEE Sensors Journal*, vol. 19, no. 6, pp. 2266–2274, 2018.

[131] V. Gupta and R. B. Pachori, "A new method for classification of focal and non-focal EEG signals," in *Machine Intelligence and Signal Analysis.* Springer, 2019, pp. 235–246.

[132] R. B. Pachori and D. Hewson, "Assessment of the effects of sensory perturbations using Fourie-Bessel expansion method for postural stability analysis," *Journal of Intelligent Systems*, vol. 20, no. 2, pp. 167–186, 2011.

[133] N. E. Huang, Z. Shen, S. R. Long, M. C. Wu, H. H. Shih, Q. Zheng, N.-C. Yen, C. C. Tung, and H. H. Liu, "The empirical mode decomposition and the hilbert spectrum for nonlinear and non-stationary time series analysis," *Proceedings of the Royal Society of London. Series A: Mathematical, Physical and Engineering Sciences*, vol. 454, no. 1971, pp. 903–995, 1998.

[134] R. R. Sharma and R. B. Pachori, "Improved eigenvalue decomposition-based approach for reducing cross-terms in Wigner-Ville distribution," *Circuits, Systems, and Signal Processing*, vol. 37, no. 8, pp. 3330–3350, Aug 2018.

[135] R. R. Sharma, M. Kumar, and R. B. Pachori, "Automated CAD identification system using time-frequency representation based on eigenvalue decomposition of ECG signals," in *Machine Intelligence and Signal Analysis*, M. Tanveer and R. B. Pachori, Eds. Singapore: Springer Singapore, 2019, pp. 597–608.

[136] A. Upadhyay, "Speech enhancement based on mEMD-VMD method," *Electronics Letters*, vol. 53, pp. 502–504(2), March 2017.

[137] R. B. Pachori and A. Nishad, "Cross-terms reduction in the Wigner–Ville distribution using tunable-Q wavelet transform," *Signal Processing*, vol. 120, pp. 288 – 304, 2016.

[138] R. R. Sharma, "Time–frequency representation using IEVDHM–HT with application to classification of epileptic EEG signals," *IET Science, Measurement and Technology*, vol. 12, pp. 72–82(10), January 2018.

[139] A. Bhattacharyya and R. B. Pachori, "A multivariate approach for patient-specific EEG seizure detection using empirical wavelet transform," *IEEE Transactions on Biomedical Engineering*, vol. 64, no. 9, pp. 2003–2015, Sep. 2017.

[140] P. Jain and R. B. Pachori, "An iterative approach for decomposition of multi-component non-stationary signals based on eigenvalue decomposition of the Hankel matrix," *Journal of the Franklin Institute*, vol. 352, no. 10, pp. 4017–4044, 2015.

[141] R. R. Sharma and R. B. Pachori, "Baseline wander and power line interference removal from ECG signals using eigenvalue decomposition," *Biomedical Signal Processing and Control*, vol. 45, pp. 33 – 49, 2018.

[142] R. R. Sharma and R. B. Pachori, "A new method for non-stationary signal analysis using eigenvalue decomposition of the Hankel matrix and Hilbert transform," in *2017 4th International Conference on Signal Processing and Integrated Networks (SPIN)*, Feb 2017, pp. 484–488.

[143] A. Bhattacharyya, "Advanced wavelet transforms based EEG signal processing methods for epilepsy diagnosis," Ph.D. dissertation, Discipline of Electrical Engineering, IIT Indore, 2018.

[144] P. Jain and R. B. Pachori, "Time-order representation based method for epoch detection from speech signals," *Journal of Intelligent systems*, vol. 21, no. 1, pp. 79–95, 2012.

[145] R. Pachori and P. Sircar, "Non-stationary signal analysis: Methods based on fourier-bessel representation," *LAP LAMBERT Academic Publishing, Germany*, 2010.

[146] G. Moody and R. Mark, "A database to support development and evaluation of intelligent intensive care monitoring," *Computers in Cardiology 1996*, pp. 657–660, 1996.

[147] W. Karlen, M. Turner, E. Cooke, G. Dumont, and J. M. Ansermino, "Capnobase: Signal database and tools to collect, share and annotate respiratory signals," in *Annual Meeting of the Society for Technology in Anesthesia (STA)*, West Palm Beach, 2010.

[148] A. Garde, W. Karlen, J. M. Ansermino, and G. A. Dumont, "Estimating respiratory and heart rates from the correntropy spectral density of the photoplethysmogram," *PLOS ONE*, vol. 9, no. 1, pp. 1–11, 01 2014.

[149] L. Cohen and C. Lee, "Instantaneous frequency, its standard deviation and multicomponent signals," in *Advanced Algorithms and Architectures for Signal Processing III*, vol. 975. International Society for Optics and Photonics, 1988, pp. 186–209.

[150] P. Sedgwick, "Pearson's correlation coefficient," *Bmj*, vol. 345, p. e4483, 2012.

[151] M. Spitzer, J. Wildenhain, J. Rappsilber, and M. Tyers, "Boxplotr: a web tool for generation of box plots," *Nature methods*, vol. 11, no. 2, p. 121, 2014.

[152] J. M. Bland and D. G. Altman, "Measuring agreement in method comparison studies," *Statistical Methods in Medical Research*, vol. 8, no. 2, pp. 135–160, 1999.

[153] J. M. Bland and D. Altman, "Statistical methods for assessing agreement between two methods of clinical measurement," *The Lancet*, vol. 327, no. 8476, pp. 307–310, 1986.

[154] R. B. Pachori, "Discrimination between ictal and seizure-free EEG signals using empirical mode decomposition," *Research Letters in Signal Processing*, vol. 2008, p. 14, 2008.